

A Jump Distance Distribution-based Bayesian model selection procedure reliably extracts molecular motion features from single molecule tracking data

Sylvain Tollis^{1,2}

¹: Wellcome Trust Centre for Cell Biology, University of Edinburgh, Michael Swann Building, Max Born Crescent, Edinburgh, EH9 3BF, United Kingdom

²: Institut de Biologie et Génétique Cellulaires, CNRS UMR5095, 1 rue Camille Saint-Saën - CS61390, Université de Bordeaux - Campus Carreire, 33077 Bordeaux Cedex, France

Correspondence : Sylvain Tollis, s.simyion@wanadoo.fr

Abstract

Single-molecule tracking (SMT) methods are under considerable expansion in many fields of cell biology, as the dynamics of cellular components in biological mechanisms becomes increasingly relevant. Despite the development of SMT technologies, it is still difficult to reconcile a sparse signal at all times (required to distinguish single molecules) with long individual trajectories, which would be required for efficient Mean-Square Displacement-based analysis, within confined regions of the cell and given experimental limitations. In this work, we develop and implement a new mathematical analysis method of SMT trajectories, which aims to take advantage of the (large) number of (short) trajectories that are typically obtained with cellular systems *in vivo*. The method is based on the fitting of the jump distance distribution, e.g. the distribution that represents how far molecules travel in a set time interval; it uses a Bayesian approach to compare plausible molecule motion and extract both qualitative and quantitative information. Finally, the method is tested on *in silico*

trajectories simulated using Monte Carlo algorithms, and ranges of parameters for which the method yields accurate results are determined.

Introduction

Recent improvements in both the spatial and temporal resolution of fluorescence microscopy imaging has allowed to detect and track individual biological molecules over time in living cells and tissues. Single Molecule Tracking (SMT) experiments have become increasingly popular, as illustrated by the attribution of the 2014 Nobel Prize of Chemistry to the pioneer work of Betzig, Hell and Moerner, in a variety of fields ranging from plasma membrane dynamics [1,2], to the high resolution imaging of internal organelles [3,4] or intracellular transport [5]. With the development of more photostable fluorophores [6-8] and increasingly sensitive cameras, applications of SMT have extended to fields as diverse as cellular neurosciences [9-11], biomedicine [12,13], or fundamental cell biological studies involving for instance the motion and spatial organization of cell surface receptors [14,15], the dynamics of transcription factors [16] or of Calcium channel receptors [17].

Super-resolution (SR) imaging and tracking of single biological molecules was initially designed to provide information on their local environment and transport dynamics. Indeed, although knowledge on the static and genetic aspects of interactions among biological molecules of interest builds rapidly, very little is known about the complementary dynamic behaviour of these molecules. SR/SMT is therefore an appealing technique to uncover the spatial and temporal regulation of individual and collective transport properties of proteins, lipids... [18-28]. The key advantage of this technique over conventional microscopy is that SMT experiments capture rare molecular events that reflect the fine features of stochastic cellular dynamics which would be averaged out in experiments returning ensemble-averaged quantities.

The drawback, however, is that inferring reliable information from single molecule trajectories requires to extract meaningful signals from stochastic molecular transport. In particular, it is crucial to develop analysis tools that fully account for trajectory variability and noise properties in transport model evaluation [18,29]. Mathematical analysis tools able to perform

this task while overcoming experimental limitations such that the sampling rate (duration of time frames), the total acquisition time, localization errors, trajectories crossing or the number of trajectories [30-32] are still to be found.

Single molecule experiments provide raw data as a time series of imaged frames. Computer algorithms are generally used to detect and localize individual molecules on each frame, and link molecules' positions in subsequent frames to track a given molecule over time, yielding single molecule trajectories. In the past decade, several research groups have developed and strongly improved powerful tracking algorithms, able to deal with fluorophore blinking, focal drift, and the merging or splitting of trajectories for instance [1,2,29,33-36]. However, owing to the limited optical resolution, it is still difficult to follow single molecules for a long time while keeping the occurrence of trajectories merging or clustering to a reasonably low level, except in artificial, controlled *in vitro* systems [37-39]. This is especially true when tracked molecules are concentrated in a specific subcellular region (organelles, liposomes, molecule clusters, polarized regions, membrane substructures ...). In addition, photo-bleaching and blinking of the fluorophores themselves introduces physical limitations to the length of acquired trajectories [36,40]. Hence, SMT strategies often yield quite short trajectories (less than 100 points) that require specific analysis methods (see [40,41] and references therein). Furthermore, biological molecules potentially experience multiple modes of transport over the course of a "long" trajectory (>1s) [42,43]. In this situation, specific analyses approaches are required to separate the different modes of transport and estimate their relative contribution on individual trajectories. How can we infer, from SMT data, the relative contributions of multiple modes of transport to the dynamics of a population of molecules despite experimental limitations?

In the last decades, many modes of biological transport have been modelled and well-characterized mathematically [44], including for instance passive diffusion through homogeneous or heterogeneous medium [45] or embedded in polymer networks [46], active motion avoiding mobile or immobile obstacles [47], or directed motion along cytoskeletal

tracks [48]. However, in practice, even in the simplest case where diffusion is essentially Brownian the interpretation and extraction of biological information is often challenging [18] [32,49]. In particular, there is currently a need for a robust analysis of short trajectories obtained from SMT experiments. Despite recent works that tackled this issue [40,41], the characterization of the underlying motion model is still broadly done through the analysis of the mean-square displacement (MSD), e.g. the Squared Displacement (SD) of the molecule between two points of its trajectory separated by a given time lag, averaged over all the points of the trajectory, plotted as a function of the time lag [10,50-55]. Molecules experiencing free Brownian diffusion yield linear MSD vs time lag plots, the slope being proportional to the diffusion coefficient D [56]. Sublinear plots indicate constrained diffusion and/or molecular interactions, while supralinear MSD indicates active transport processes [56,57]. The key limitation of the MSD analysis is that fluctuations of the SD increase with the time lag, especially when the latter represents a significant fraction of the entire trajectory; for short trajectories, this statistical noise affects all the points of the MSD vs time lag plots, making the determination of the motion parameters inaccurate. For instance, the distribution of short range diffusion coefficient calculated from short trajectories is so wide that measurements become useless [58,59]. A minimal number of 100-1000 trajectory points seem to be typically required for meaningful MSD analysis [32,60], which is hard to achieve experimentally. Ensemble averaging of individual MSD curves usually damps the fluctuations and improves the accuracy of the diffusion coefficient determination [32]. However, if multiple transport modes are present, ensemble-averaging tends to average out the less frequent transport modes to the benefit of the dominant transport mode, whose measured parameters are slightly altered owing to contributions of the other modes [42,61]. Despite these limitations, MSD-based analysis of SMT data is still widely used, both in mammalian cells [62], yeast [54] or other model organisms like *C. elegans* [63] [64]. How can ensembles of short trajectories be analyzed to extract meaningful information?

Alternative measurable quantities have been considered to analyze molecular transport in living cells. Among them, the Mean Maximal Excursion [41] and Jump Distance Distribution (JDD) provide promising alternatives to the MSD [65-72]. The jump-distance (JD) is defined as the distance travelled by a single molecule during a fixed time lag τ . The distribution of these jump distances over a large population of molecules is characteristic of the underlying transport mode(s) and quantitative features, and of the time lag. The JDD analysis takes advantage of the fact that modern, powerful imaging systems and tracking algorithm produce generally a large number of individual trajectories allowing to plot well-resolved JD distributions. There exist closed-form mathematical formulations of JDDs for many motion models [56,69,73]; conveniently, JDDs for composite populations encompassing molecules experiencing different transport modes can be easily obtained by multiplying the JDD of each mode by the fraction of molecules affected and summing the contributions of all subpopulations (see Materials and Methods, M&M). To calculate the JDD, all trajectories must be of same duration τ , which is achieved by splitting longer trajectories into sub-trajectories of duration τ that will be considered as an individual trajectory. This procedure naturally separates multiple transport modes that may be experienced by a single molecule along its entire trajectory. It is clear that in principle the JDD analysis should overcome two of the major limitations of *in vivo* SMT, e.g., short trajectories, and possible multiple motion modes, to the detriment of losing single-trajectory information. Motion parameters, such that the diffusion coefficient, are therefore obtained at a population level. This method has been already used successfully in various contexts [9,68,69]. However, fitting the JDD obtained from *in vivo* data requires the knowledge of an underlying motion model *a priori*, which is in general unknown. Then, multiple motion models can lead to satisfactorily fits of the experimental data, hence the requirement for a model selection procedure.

Model selection can be achieved through the minimization, with respect to model parameters, of the mean squared error between experimental data and model prediction for a given quantity (such that the MSD, JDD ...). Models can be classified according to their

least square difference to the experimental data, a smaller error being interpreted as a better model. This procedure generally selects overly complex models (with more parameters), which usually produce better fits, while the particular features of a given measurement might only reflect stochastic variations of a simple underlying transport mechanism [32,44,58,74]. Getting biophysical insight on molecular mechanisms from SMT is a matter of great debate in the community, as there is no consensus on the best method to extract meaningful information. Various methods have tackled this problem in the past few years, via for instance the definition of adequate information criteria [75] or maximal likelihood estimators [40], or the use of probabilistic graphical models [76]. Recently, approaches based on Bayesian inference have been introduced to discriminate between competing motion models [75,77-80]. The Bayesian inference method evaluates the likelihood of a given underlying motion model given a set of measured quantities, and has proven successful in handling noise and experimental limitations in other biological applications including fluorescence correlation spectroscopy [76,81-85]. However, to the best of our knowledge, Bayesian methods for motion model inferring from SMT data have been mostly restricted to the MSD-based analysis, and might therefore be inaccurate to analyze short trajectories and/or long trajectories encompassing multiple transport modes [18,44,74,77].

In this article, we derive a Bayesian approach for motion model selection, based on the fitting of the Jump Distance Distribution. Our procedure yields probabilities of tested models to be the “true” underlying motion model, given an actual experimental JDD. We demonstrate mathematically that for typical SMT experiments, those probabilities can be calculated by integrating motion model probabilities over a narrow subregion of their parameter space, centred around the set of model parameters that minimize a generalized least squared error function (see M&M for details). Integration over the parameter space is crucial to deal with the uncertainty on model parameter measurement that arise from biological noise, and was shown to favour simple models to the detriment of overly complex models [77]. To test the reliability of our approach and estimate its accuracy, we perform model parameters

determination and model selection on sets of trajectories simulated using Monte Carlo methods for free diffusion (model D), anomalous diffusion (model A), noisy directed motion (model V), and composite models encompassing two subpopulations of trajectories corresponding to different motion modes (models DD, DV, DA), with simulation and motion parameters varying over orders of magnitude. For each model and set of parameters tested, 20 JDDs were generated, analyzed via our generalized least square fitting approach, yielding an estimate of the typical error that may be expected when measuring model parameters. This error was used to define a “confidence range” for each parameter measured by least square fitting for each model. Numerical integration of model probabilities over parameter values within their respective confidence range allows to average out the effects of stochastic variations on model parameters determination and to estimate the overall model probability given the observed JDD, reducing the risk of selecting overly complex models, a general property of Bayesian inference [77-80,84-86].

The paper is organized as follows: first, we use simulated JDDs to systematically determine the accuracy of parameter determination as a function of trajectory length, number of JDD bins, number of simulated trajectories, and model parameters for all 6 models introduced above. We show that our fitting procedure is accurate for all motion models and for large parameter ranges, even for short trajectories, and we determine the parameter ranges under which the accuracy is reduced. Then, for particular sets of biological parameters representative of these ranges, we estimate the accuracy of the JDD-based Bayesian model selection procedure and show that composite populations are correctly identified in biologically-relevant situations.

Results

Characterizing single molecule transport using the Jump Distance Distribution

The method described in this article was developed to analyze a set of N individual planar trajectories, or fraction of trajectories, labelled with the index $j = 1..N$. All trajectories are assumed to have an identical duration $\tau = M\delta t$ and comprise of $M + 1$ points of planar Cartesian coordinates x_j^p and y_j^p , $p = 1..M + 1$; δt is the time step between two consecutive measurements of single molecules' positions. For each trajectory, the jump distance, e.g. the geometrical distance between its first and last points, is defined by:

$$l_j = \sqrt{(x_j^{M+1} - x_j^1)^2 + (y_j^{M+1} - y_j^1)^2} .$$

The experimental jump distance distribution (JDD) is defined by classifying the N jump distances in N_b ordered bins of fixed size (see Figure 1A and M&M for details). The distribution is therefore defined by the set of integer numbers $\{N_i, i = 1..N_b, \sum_{i=1}^{N_b} N_i = N\}$ corresponding to the number of trajectories in each bin for the analyzed dataset.

To illustrate the power of the method, we have chosen to fit this experimental JDD with 6 two-dimensional motion models which correspond to established biological transport modes [10,43,57,62,87]: a free diffusion model, denoted with the letter 'D' in the following, characterized by a single parameter, the diffusion coefficient D ; a noisy directed motion model, denoted with the letter 'V', parametrized by the velocity V of the directed transport along linear tracks and the variance k_V of the molecule position at each step around its mean position governed by the directed motion [5,43]; a model of anomalous (sub)diffusion, denoted with the letter 'A' and parametrized by the anomalous diffusion coefficient D_α and the power exponent $\alpha < 1$ [56,88,89]; and finally 3 composite models, encompassing a fraction f_D of molecules transported through free diffusion and a fraction $1 - f_D$ that follows either free diffusion with a larger diffusion coefficient D_2 (model 'DD'), or directed transport

(model 'DV') or anomalous subdiffusion (model 'DA') ; these composite models are characterized by the parameters needed for each submodel in addition to the fraction f_D .

Mathematical closed form expressions for the probability for a molecule to jump a distance r_i during the time τ have been derived for various motion models in the past (jump distance probability, see M&M), including free diffusion with or without a linear bias corresponding to directed motion, confined diffusion [73], anomalous subdiffusion [56,90] or superdiffusion [91] including with Levy flights [92]. The theoretical jump distance distributions $\{\tilde{N}_i^{D,V,A}, i = 1..N_b\}$ are easily obtained by multiplying the probabilities by the number of molecules. Figure 1B shows that long tails in the JDD (e.g., longer than for pure Brownian motion, dashed black curve) can be the consequence of both a faster (pure) diffusion (dark blue), directed transport (green), or anomalous diffusion (red). Generally speaking, anomalous subdiffusion tends to be characterized by a main peak shifted towards the small distances in the JDD, while the tail at large distances is enhanced and extended compared to pure diffusion. In contrast, directed transport is characterized by a Gaussian-like peak, whose peak distance increases linearly with the transport velocity, and the spreading characterizes the (positional) noise in the directed motion.

The theoretical JDD for models mixing two subpopulations of molecules including a fraction f_D of molecules diffusing freely are readily obtained:

$$\tilde{N}_i^{DD,DV,DA} = f_D \tilde{N}_i^D + (1 - f_D) \tilde{N}_i^{D_2,V,A} ,$$

In the following, we show that model optimization, e.g. the search for model parameters that correspond to the maximum likelihood of observing the actual experimental data given a putative motion model X, is obtained through the minimization of the generalized squared error $\sum_{i=1}^{N_b} w_i (\tilde{N}_i^X - N_i)^2$ with some specific weights w_i that we derive analytically.

Bayesian approach for model selection on JDD data

For K competing models M_k (here, $K = 6$, $k = 1..K$), and a set of observed data $\{N_i\}$, the probability of each model to be the actual underlying motion mode that produced $\{N_i\}$ is given by the Bayes theorem [77]:

$$P(M_k|\{N_i\}) = \frac{P(\{N_i\}|M_k)P(M_k)}{\sum_{k=1}^K P(\{N_i\}|M_k)P(M_k)}$$

With no a priori knowledge on the underlying motion model, which is generally the case when SMT analysis begins, all the models considered are equiprobable *a priori*. In this case, the latter expression simplifies to:

$$P(M_k|\{N_i\}) = \frac{P(\{N_i\}|M_k)}{\sum_{k=1}^K P(\{N_i\}|M_k)}$$

Where the marginal probability $P(\{N_i\}|M_k)$ is obtained by expanding over the model parameter space:

$$P(\{N_i\}|M_k) = \int P(\{N_i\}|M_k, \beta_k)P(\beta_k|M_k) d\beta_k$$

Here, β_k denotes the entire set of model parameters. The way $P(\beta_k|M_k)$ is estimated is detailed in M&M.

To calculate $P(\{N_i\}|M_k, \beta_k)$, we assume that the jump distance for different trajectories are independent random variables. Given a motion model M_k with its parameters β_k , for a single trajectory of duration τ the probability p_i that the jump distance falls in the i^{th} bin is, by definition, deduced from the JDD of the corresponding model:

$p_i = \frac{\tilde{N}_i^{M_k}}{N}$. Since the jump distances of different trajectories are assumed to be independent

variables, the probability $P(\{N_i\}|M_k, \beta_k)$ satisfies a multinomial distribution:

$$P(\{N_i\}|M_k, \beta_k) = \frac{N!}{N_1! N_2! \dots N_{N_b}!} p_1^{N_1} p_2^{N_2} \dots p_{N_b}^{N_{N_b}}$$

with the usual constraint $\sum_{i=1}^{N_b} N_i = N$, and where the probabilities p_i depend on the model and its parameters. Although exact, this expression is untractable in numerical computations, so we proceeded to approximate $P(\{N_i\}|M_k, \beta_k)$ using the Stirling formula to express factorials, followed by a Laplace saddle-point approximation. Details of the calculations are provided in M&M, and we readily obtain:

$$P(\{N_i\}|M_k, \beta_k) \sim \frac{\sqrt{2\pi N}}{\prod_i \sqrt{2\pi N p_i}} e^{-\frac{N}{2} \sum_{i=1}^{N_b} \frac{(y_i - p_i)^2}{p_i}},$$

where $y_i = N_i/N$ represents the experimental data, the reference probabilities p_i depend on the model M_k and its parameter(s) β_k .

As a first consequence of this latter expression, for each model M_k the parameters β_k that maximize the likelihood of the observed configuration are those which minimize the generalized squared error $\sum_{i=1}^{N_b} w_i (y_i - p_i)^2$ where the squared error at each point is weighted by the inverse of its variance $w_i = 1/p_i$. To the leading (second) order in $y_i - p_i$ we can set $w_i = 1/y_i$ and the weights are then independent on model parameters. The minimization of $\sum_{i=1}^{N_b} w_i (y_i - p_i)^2$ is then performed using standard weighted least squares method based on the Newton-Gauss algorithm. This procedure yields a set of optimal parameters β_k^0 that maximize the likelihood of observing the jump distance distribution that was actually observed given a specific model, and can therefore be interpreted as the *measured model parameters* (see [77]).

Owing to the stochastic nature of molecular transport, parameters measurements have a limited accuracy, and the measured parameters β_k^0 might deviate from the “true” *in vivo* value by some uncertainty $\delta\beta_k$. In other words, a finite sample of ~ 1000 trajectories for instance can seem to diffuse faster than another sample from the same cell collected over the same period of time. The Bayesian method allows managing uncertainties with scientific insight.

Following the procedure described in [77], we used uniform prior distributions for $P(\beta_k|M_k)$ within a certain range $\beta_k^{min} \leq \beta_k \leq \beta_k^{max}$ and $P(\beta_k|M_k) = 0$ elsewhere; thus the integration over parameters β_k represents a simple averaging of the peaked probability $P(\{N_i\}|M_k, \beta_k)$ over an integration range $[\beta_k^{min}, \beta_k^{max}]$ defined as a symmetric interval centred in β_k^0 , the maximum likelihood estimation of β_k , and with a width proportional to the uncertainty $\delta\beta_k$ on parameter determination. This procedure provides an opportunity to penalize models with too many parameters, and also models for which parameters may be measured inaccurately. In summary, with $P(\{N_i\}|M_k, \beta_k)$ defined analytically and $P(\beta_k|M_k)$ defined using adequate integration boundaries, the marginal probabilities of each tested model are completely known.

To estimate both the accuracy of parameters measurements on which the method relies, and the uncertainties $\delta\beta_k$ that define the integration ranges, we have performed generalized squared error minimization on simulated trajectories.

Monte Carlo Simulation of single molecule trajectories

Planar single molecule trajectories were simulated using in house Matlab (Mathworks) scripts (see M&M). Free diffusion was simulated by a two dimension random walk with fixed time steps $\delta t = 20ms$, in agreement with the typical time resolution of SMT experiments [54], and space steps sampled from a Gaussian distribution of variance $2D\delta t$ in both directions of space, where D is the diffusion coefficient. Directed motion (model 'V') was simulated using the same fixed time steps and space steps comprising of a linear jump of length $V\delta t$ in a random direction and a random step sampled from a Gaussian distribution of variance k_V in both directions of space to account for positional noise along the directed motion tracks. Anomalous subdiffusion was simulated using a Continuous Time Random Walk [56]. Waiting times between steps were sampled from a distribution comprising a short tail at short times $t < \delta t' = 0.01ms$ and a long Pareto-like tail at larger times, while space steps were sampled from a Gaussian distribution of variance $2D_\alpha\delta t'^\alpha$ in both directions of space [56]. This

algorithm, with long tailed waiting times distributions, yields anomalous diffusion at large times τ [93]. This is due to an overall balance between molecules having significant probabilities both to wait for long times without moving or to do many Brownian moves in a short window of time, yielding a JDD that is shifted towards smaller distances but also includes a longer tail towards large distances compared to free diffusion (Figure 1B).

Composite models ('DD', 'DV', and 'DA') were simulated by choosing the motion mode randomly for each simulated molecule, with a probability f_D for free diffusion. Hence, two simulations with the same parameter f_D can have slightly different numbers of freely diffusing molecules, as expected from the stochastic observation of a part of the total pool of molecules *in vivo*.

An overall working precision of 10^{-6} was chosen for numerical computations, in particular to calculate the generalized squared error $\sum_{i=1}^{N_b} w_i (y_i - p_i)^2$ and to calculate integrations over the parameter space using Simpson quadrature in Matlab (routine `quadv`). This choice represents a compromise between the large CPU time needed for high precision computations and the requirement that the numerical error on $\frac{N}{2} \sum_{i=1}^{N_b} w_i (y_i - p_i)^2$ is much smaller than unity, with typically $1000 < N < 10000$. The influence of the number of bins N_b , motion model parameters and the time lag (e.g., the number of trajectory points) on model parameters determination is analyzed below.

Performance of parameters measurement on simulated trajectories

For each model and parameter set, a total of 20 simulations (*in silico* experiments) were performed. Unless otherwise specified, the following parameters were used for each *in silico* experiment:

- Trajectories and analysis parameters: $N = 3000$, $N_b = 30$, $\tau = 0.14s$
- Motion models parameters: $D = 0.02 \mu m^2/s$, $V = 1.2 \mu m/s$, $k_V = 0.0008 \mu m^4/s^2$, $D_\alpha = 0.02 \mu m^2/s^\alpha$, $\alpha = 0.5$, and $f_D = 0.5$.

Examples of simulated trajectories are shown on Figure 1A. Since our purpose is to demonstrate that our method is efficient to extract relevant information from short trajectories, we have chosen to use the default time lag $\tau = 0.14s$ that, given our time resolution, corresponds to trajectories of only 8 points, throughout the study, unless otherwise specified.

The JDD produced by each *in silico* experiment was analyzed using a fitting algorithm based on the Gauss-Newton method, which finds the minimum of the generalized squared error function $\sum_{i=1}^{N_b} w_i (y_i - p_i(\beta_k))^2$ by slightly modifying the parameters β_k iteratively along the gradient of the function, which is recalculated at each iteration. Starting values for the parameters β_k were estimated automatically from the localization of the peak(s) in the JDD. The convergence of the algorithm was decided as soon as the relative change in generalized squared error $\sum_{i=1}^{N_b} w_i (y_i - p_i)^2$ between two successive iterations was less than the working precision. This condition was not always achieved, owing to the oscillatory behaviour of some fitting functions and numerical uncertainties. In this case, a maximal number of iterations of 100000 (models 'D', 'V', 'DD', 'DV') or 5000 (models 'A', 'DA') was used instead, and convergence was visually checked. Computations were performed on a MacBook Pro laptop hosting a 2.53 GHz (P8700) Intel Core 2 Duo CPU.

Results of these tests are displayed on Figure 2, where the relative error to which model parameters are measured is shown as a function of N_b with constant N (2A), N_b with constant N/N_b (2B), time lag (2C), and model parameters (2D), for the models D, V, and A. Figure 2A shows that increasing the number of bins while keeping the number of trajectories constant decreases the accuracy of the optimal diffusion coefficient, both for D and A models. This is a consequence of the statistical noise in the distribution of jump distances, that becomes predominant when the condition $N/N_b \gg 1$ is not fulfilled. In contrast, the velocity parameter is measured with a great accuracy over the entire range of bin numbers for the V model. Figure 2B shows that, in contrast, increasing the number of bins while

keeping the ratio N/N_b constant was less affecting the estimated diffusion coefficient. This demonstrates that increasing the resolution of the JDD (number of bins) without reducing the accuracy of the fitting procedure can be done by simply increasing the number of trajectories, which is always possible, at least technically. In addition, Figure 2C shows that, for the default parameters chosen in this study, the time lag, or equivalently here the number of trajectory points, does not influence the accuracy of parameter determination for the non-composite motion models. Finally, Figure 2D shows that broad ranges of motion model parameters are measured with a typical accuracy of less than 10%, even for the very short 8-points trajectories simulated for testing the method, confirming that the JDD is an excellent measurable quantity to characterize molecular transport with the typical experimental limitations. It is noteworthy that the fitting accuracy is significantly decreased for very low directed transport velocities (green line) and anomalous diffusion with large power exponent α (dashed magenta line), where, respectively, transport is dominated by the diffusion-like noise term and the anomalous character vanishes ($\alpha = 1$ represents pure diffusion). Thus, regimes where parameters of the A and V models are less well determined correspond to parameter regimes where these models behave as pure diffusion. In contrast, the anomalous power exponent α is measured more accurately in this large α regime (Supplementary Figure S1).

Then, we estimated the ability of the least squares parameter measurement procedure to accurately separate contributions from subpopulations experiencing different modes of transport in a given realization of the JDD. In this purpose, we performed Monte Carlo simulations of composite models, computed the simulated JDDs and fitted them with the closed form expressions for the theoretical JDDs given previously. Results of these tests are displayed on Figure 3 for the DD model (3A), DV model (3B) and DA model (3C). Figure 3A shows that the contributions of two subpopulations of freely diffusing molecules with different diffusion coefficients D_1 and D_2 can be reliably distinguished (error on their relative fraction less than 0.2, red and blue regions of the diagram) whenever $D_{2(1)} > 2 - 3D_{1(2)}$ (left panel).

Therefore, in practical applications, it will be possible to distinguish organelle-bound proteins (with typical diffusion coefficient $D_1 < 0.1 \mu\text{m}^2/\text{s}$) from cytosolic proteins (with typical diffusion coefficient $D_2 > 1 \mu\text{m}^2/\text{s}$). As for the simple models, increasing the bin number without increasing the number of trajectories used to build the JDD is detrimental to the fitting accuracy (right panel, black line), while it does not significantly affect the error on subpopulation fractions when the number of trajectories is also increased (light grey). Furthermore, modifying the time lag does not change the fitting accuracy in this situation (dark grey). It is noteworthy that this right panel was obtained with $D_1 = 0.02 \mu\text{m}^2/\text{s}$ and $D_2 = 0.1 \mu\text{m}^2/\text{s}$, e.g. in a parameter regime where the subpopulation fractions are accurately measured using the default parameters (see left panel). In contrast, increasing the number of bins (and, together, the number of trajectories), might be useful to discriminate between two subpopulations with quite similar diffusion coefficients (data not shown). Similarly, Figure 3B (left panel) shows that two subpopulations experiencing respectively pure diffusion and (noisy) directed transport can be generally distinguished with a high accuracy (error on their relative fraction less than 0.2, red and blue regions of the diagram). For a diffusion coefficient $D = 0.01 - 0.04 \mu\text{m}^2/\text{s}$, consistent with *in vivo* measurements on membrane-associated proteins [55] [63], directed transport can be identified as soon as the transport velocity exceeds $0.5 - 0.7 \mu\text{m}/\text{s}$, which is in the range of myosin motor proteins-mediated transport velocity [94] [43]. This accuracy decreases for larger $D = 0.08 - 0.15 \mu\text{m}^2/\text{s}$, a regime relevant in some biological contexts [10]; in these cases, subpopulation fractions are well determined only for $V > 1 - 1.5 \mu\text{m}/\text{s}$ (for our default analysis parameters), requirement that is also achieved *in vivo* [94]. In addition, the Figure 3B right panel shows that increasing the time lag (dark grey) improves the determination of the subpopulation fractions very significantly were we to distinguish fast diffusion from slow active transport. This reflects a simple scaling argument: the position of the diffusion and directed transport peaks in the JDD scale with the square root of the corresponding MSD with a timeshift equal to the chosen time lag τ , respectively $\sqrt{\tau}$ and τ . Thus, increasing τ tends to separate these peaks, and

therefore the contributions of the two subpopulations to the JDD, which makes them easier to identify. Surprisingly, increasing the number of bins didn't improve the fitting accuracy (black, light grey). Finally, we analyzed the ability of the generalized least squares fitting procedure to separate the contributions of pure and anomalous diffusion in a composite DA simulated JDD. Similarly to the tests performed on DD and DV models, Figure 3C (left panel) shows that freely and anomalously diffusing subpopulations can be distinguished accurately as soon as the diffusion and anomalous diffusion coefficients are significantly different (error on their relative fraction less than 0.2, red and blue regions of the diagram). In contrast with the DD model though, where the "worst case scenario" is achieved when $D_1 \sim D_2$, the $D - D_\alpha$ parameter range for which the subpopulation fractions are inaccurately measured depends on the anomalous power exponent α . Figure 3C shows that for $\alpha = 0.5$, the fractions are more likely to be well determined for $D < D_\alpha$, $D \sim D_\alpha$ and $D \gg D_\alpha$ (see left of the diagram), while for $D \geq D_\alpha$ the peaks corresponding to the two subpopulations overlap and parameter measurement is less accurate. Contrary to the DV model, increasing the time lag is detrimental to the fitting accuracy (see Figure 3C, right, dark grey). As described for other models, increasing the number of bins (for instance, to discriminate between two subpopulations whose peaks in the JDD partially overlap) tends to reduce the accuracy in the other parameter ranges (black line). As previously, increasing the number of trajectories as well restores partially the accuracy of the fractions determination (light grey line).

In summary, we have proven that automated least squares-based fitting of simulated JDD reliably extract the fraction of two subpopulations for the composite models DD, DV, and DA, over broad ranges of parameters. For composite models, the total JDD is the sum of individual models JDDs, weighted by the fraction of each subpopulation in the total population. Therefore, the overall JDD might exhibit one or two distinct peaks depending on how different the subpopulations motion parameters are. While it might be required to increase the number of bins to resolve close peaks, this operation generally increases the noise of the JDD (as each bin "contains" a smaller number of trajectories), and therefore

reduces the fitting accuracy if the peaks are resolvable. Thus, an optimal number of bins might be required, depending on the ranges of motion parameters. Increasing the number of trajectories improves the accuracy for a larger number of bins. Furthermore, while increasing the time lag allows separating free diffusion from directed transport, it is generally detrimental if one wants to resolve free from anomalous diffusion, indicating that an optimal time lag might also be required.

How well are motion parameters measured for the simulated composite models? For all the parameter ranges shown on Figure 3 (bins number with or without different number of trajectories, time lags, simulated motion parameters), and for different input fractions in the simulated population, the automated least squares fitting provided estimates of the underlying motion parameters. However, owing to the large number of simulations performed, we chose not to represent the relative error on measured parameter as a function of all other parameters as this would have yielded dozens of plots similar to Figure 2, and blurred the main message. Instead, we generated scatter dot plots showing, for each composite model, the relative error on measured parameter as a function of the error on the estimated subpopulation fraction for the same simulated JDD (see Figure 4). These plots show that, in most cases, motion parameters are reliably measured (relative error less than 0.2, vertical axis) when the subpopulations fractions are also accurately determined (error less than 0.2, horizontal axis). Thus, conclusions drawn on the ability of the least squares fitting to distinguish between subpopulation fractions (Figure 3) generally extend to the estimation of underlying motion parameters. In contrast, situations where the method is unable to determine the fraction often correspond to an erroneous measurement of motion parameters. This is especially true for the determination of the free diffusion coefficients, (Figure 4A-C, light blue and Figure 4A, dark blue), directed transport velocity (Figure 4B, dark green) and anomalous diffusion coefficient (Figure 4C, magenta). The positional variability parameter k_V for the DV model (Figure 4B, light green) and the anomalous power exponent for the DA model (Figure 4C, orange) are more likely to carry

larger errors despite an accurate determination of the subpopulation fraction. In agreement with the conclusions of [69], for uneven composite simulated subpopulations the motion parameters are always well determined for the dominant fraction, with a relative error smaller than 0.3 in the worst case scenario (Figure S2). In addition, the error on most motion parameters decreases with an increasing fraction of the corresponding subpopulation (free diffusion coefficients D for all DD, DV, DA models in light and dark blue, anomalous power exponent for the DA model in orange and, to a lesser extent, transport velocity V for the DV model in dark green). Thus, the method yields an accurate determination of motion parameters for the dominant fraction of a composite population, which is further improved as the fraction becomes more dominant.

In addition to providing a significant test of the reliability of JDD fitting to estimate parameter values for several motion models, this first series of tests allowed to estimate the accuracy level to which a given motion model parameter can be measured by the generalized least square fitting, in presence of statistical noise. For each model parameter β , the value $\bar{\beta}$ measured by the least square analysis averaged over 20 *in silico* experiments was compared to the simulated value β_0 . For each parameter β , the typical amplitude of the difference $|\bar{\beta} - \beta_0|$ was used to define the range for integration of model probabilities over model parameters, as detailed in [77]:

$$\beta^{min,max} = \beta_0 \pm 10|\bar{\beta} - \beta_0| .$$

With these estimates in hand, *in silico* tests of the reliability of the JDD-based Bayesian method for model selection could be performed.

Performance of Bayesian model selection on simulated trajectories

In the previous section, we determined the accuracy of fitting the JDD with a given motion model. However, when analyzing actual data, most of the time there is little – if any – knowledge on the underlying motion model. How must different fits with different possible

motion models be compared, and how can we determine the motion model that is most likely to have generated the observed data? The Bayesian model selection procedure described above was next tested, with test results represented on Figures 5 and S3. In this purpose, for each motion model discussed in this article, and for motion parameters representative of the different parameter ranges discussed in the previous section, 10 JDDs were simulated and analyzed with the Bayesian model selection procedure together with parameter fitting (as described in M&M). This analysis yields, for each of those 10 runs, a probability that each tested model is « true ». When no model got a probability larger than 75%, the run was counted as « undetermined ». The output of this analysis was represented as bar charts showing the occurrence, over 10 runs, of determined motion models for each input model and parameter range. Figure 5A shows that irrespective of the diffusion coefficient, free diffusion is rarely mistaken with other types of transport (first two bars from left to right). In the presence of low to moderate noise, pure V model is also well determined (third and fourth bars), although it might be, in the small velocity regime, interpreted as a DV with a very small freely diffusing subpopulation, comparable with the typical error on f_D in this parameter regime (Figure 3B left panel). Thus, after qualitative inspection of the result, the analyst still recognizes a pure directed transport model. Similarly, significant subdiffusive character (small α) is accurately extracted, though the DA model does not seem strongly penalized by the selection procedure so that a simple A model might be mistaken with a DA model with small f_D , comparable to the typical fitting error. Here again, qualitative inspection of the result is sufficient to recover the actual nature of the underlying motion (pure A model). Our Bayesian model selection procedure is even more efficient when applied to JDDs simulated using composite models. Indeed, in the parameter regimes where f_D and motion parameters are very well determined by the automated least square fitting, the right model is determined in almost 100% of the test runs (Figure 5B). It is noteworthy that in the motion parameter regimes where the least squares fitting procedure does not provide accurate values for the parameters, the Bayesian selection procedure can lead to significant deviations between the simulated and estimated models (Figure S3). In some cases, increasing the number of bins

(and the number of trajectories) significantly improves motion model determination (V model with large V and high noise, A model with large D_α large α) ; in contrast, in other cases (V model with small V and high noise, A model with small D_α and large α) there is an apparent strong contribution of free diffusion that do reflect the fact that slow directed transport might be drowned in high noise (Figure S3A, small V /high noise and S3B, large gap high noise), while a weak anomalous character ($\alpha \sim 1$) might be underestimated (Figure S3A, small D_α large α), or even missed (see model DA, large gap large α on Figure S3B).

Discussion

Single Molecule Tracking experiments offer, in principle, the possibility to probe the local environment of molecules of interest, and therefore to gain considerable insight on their individual motion, interactions, and overall intracellular dynamics. For these reasons, SMT is increasingly used in a variety of biological contexts [11,13,16,62,63,95,96] [63]. However, despite recent progress in fluorophores engineering [97,98] and tracking algorithms, it is still difficult to follow single molecules for a long time while keeping photo-bleaching, trajectories merging or clustering to a reasonably low level, especially when the labelled molecules are clustered in small subcellular regions. Hence, the trajectories obtained are usually short, and in this limit current analysis methods fail to accurately determine motion features [32,40,41,60]. In addition, we still lack a method suitable to discriminate between multiple transport modes experienced by a single molecule along an individual trajectory.

In this work, we have derived a new method to analyze quantitatively SMT data and extract key motion features and parameters. The method was carefully derived mathematically from rigorous statistical considerations on a variable directly measurable from individual trajectories, the Jump Distance (Figure 1) [69]. We show that combining an analytically derived generalized least squares fitting of the Jump Distance Distribution by particular motion models with a Bayesian model selection procedure, offers a good alternative to Mean Square Displacement-based analysis that is also efficient for short trajectories, where the latter fails [32]. By taking advantage of the (large) number of (short) trajectories that are typically obtained with cellular systems *in vivo* to the detriment of losing single-trajectory information, the JDD analysis overcomes the experimental limitations of SMT listed above. Specifically, we first performed generalized least square fitting of simulated JDDs corresponding to uniform populations experiencing free diffusion (model D), anomalous diffusion (model A), or noisy directed motion (model V), and to composite populations encompassing two subpopulations with different motion modes (models DD, DV, DA), over a broad range of motion and trajectory parameter values. We showed that in most parameter

regimes, measurements of the input motion parameter values were accurate, with typically less than 20% error using realistic trajectories length and number. The fitting method was efficient both for uniform and composite populations (Figures 2-4 and S1-S2). In both cases, the Bayesian model selection procedure was able to determine the underlying motion mode(s) from almost all simulated JDDs (Figure 5). Note that parameters relative to anomalous diffusion were overall measured with less accuracy than for other motion modes. This may be attributed to the fact that the closed form formula for the anomalous jump distance probability was derived for Continuous Time Random Walks in the limit of infinitely small space-time steps. As a consequence, a finite trajectory consists in an infinitely large number of steps, which allows an accurate sampling of the entire distribution of waiting times. However, in practice CTRWs were simulated with finite steps, leading to an incomplete sampling of the distribution of waiting times and to sensible differences in the low distance end of the simulated JDD compared to the ideal one. Improving the simulation algorithm for anomalous diffusive motion would strengthen the tests of our analysis method.

We also identified parameter regimes in which the subpopulation fractions of composite trajectory samples were less accurately extracted (Figures 2-4). This yielded significant deviations between the simulated transport mode and the determined transport mode (Figure S3). For clarity and conciseness, we obviously couldn't report tests of all possible parameter values; however, our analysis was sufficient to extract general trends on how to use our JDD-based Bayesian method to analyze real samples, depending on the information or insight we have on the system. This « cooking recipe » is explained below.

The JDD of a uniform population has a peak, whose position scales as $\sqrt{MSD(\tau)}$, where τ is the (chosen) time lag. Different motion modes correspond to different dependence of the MSD on τ [77]: thus, for free diffusion the peak position scales as $\sqrt{D\tau}$, while for anomalous diffusion it scales as $\sqrt{D_\alpha\tau^\alpha}$ and for directed transport, as $V\tau$. Discriminating between different subpopulations will be easier for well separated peaks, and therefore distinguishing directed transport from free or anomalous diffusion will require larger time lags, while

distinguishing free from anomalous diffusion will necessitate either large or short time lags (regimes where the functions $\sqrt{\tau}$ and $\sqrt{\tau^\alpha}$ diverge from each other). Tuning the time lag can be achieved both by choosing the frequency of imaging, and by selecting the adequate number of points in the trajectories (or fractions of split trajectories). Once the time lag is chosen, the obtained JDD extends over a given range of jump distances: the choice of the number of bins depends then on this range and on the resolution needed to resolve the different peaks, making sure that there is, on average, at least 100 trajectories per bin in the sample to prevent noise in the distribution.

The methodology detailed above and in the article can be straightforwardly applied to a broad range of systems, including in vitro experiments. In addition, the analytical formulation of the method can be formally extended without new derivation to include any kind of motion mode for which there exist a closed form expression for the jump distance probability distribution $\{p_i\}$, like for instance confined diffusion [73], fractional diffusion [90] or superdiffusion [91] including with Levy flights [92]. We have restricted the numerical tests to D, V, and A motion modes only for conciseness, and because of their relevance for proteins, or lipid vesicles, moving in heterogeneous media [89,99] and their established contribution to cellular dynamics [10,43,57,62,87]. Note that strictly speaking, the method is limited to trajectory sets where the jump distances of individual trajectories are statistically independent variables (uncorrelated). This would, for instance, not be the case if a given set includes the trajectories of two interacting proteins imaged at the same time (like for instance a dimer where the two monomers are simultaneously visualized). However, the use of switchable fluorophores (like the mEOS) for which a very small number of molecules are simultaneously visualized limits the probability of observing correlated motions. Correlations might also appear when short trajectories are obtained from the splitting of long non-markovian trajectories. In this case, correlations extend over a certain fraction of the entire trajectory (the length of the « memory » kernel), and therefore increasing the time lag (the number of

points on the individual trajectories) above the correlation length should limit correlation effects.

Finally, the method can be readily extended to include composite populations encompassing 3 or more motion modes; this would require adding new terms to the linear combination defining jump distance distributions for composite models, with new subpopulation fractions as additional parameters. The projected creation of a user friendly interface that will allow the user to choose the motion modes to include, the number of subpopulations to search for and the expected ranges of motion parameters will make the method accessible to a broader audience.

Acknowledgements

We thank Derek McCusker for initiating this project and careful reading of the manuscript. We also thank Mike Tyers and Eric Schirmer for advice and complementary funding. This work was funded by in France by the Agence pour la Recherche sur le Cancer (ARC grant PDF20120605172) and CNRS, and in the UK by the Wellcome Trust Centre for Cell Biology and the University of Edinburgh.

Figure legends

Figure 1: Construction of the Jump Distance Distribution. (A) Examples of planar single molecule trajectories of equal duration (or, equivalently, number of points), gathered to the same starting point. Shown are trajectories from simulated free diffusion (black, blue for respectively slow and fast diffusion), anomalous subdiffusion (red), and noisy directed motion (green). From the unique starting point of the trajectories, circular bins are plotted (bins of size δr around $r_i, i = 1..N_b$), and trajectories are classified in the bins according to the position of their ending point, yielding the Jump Distance Distribution (see M&M). (B) Examples of JDDs obtained for a homogeneous population of freely diffusing molecules (black), and composite populations including freely diffusing molecules and: anomalously diffusing molecules (red), another pool of fast freely diffusing molecules (blue), and molecules transported along (noisy) linear tracks (green). Although these three transport modes all contribute to a long tail in the JDD, they provide unique, characteristic features that allow their distinction.

Figure 2: Automated least squares fitting of the JDD reliably extracts molecular motion parameters. Relative error on measured motion parameters as a function of the number of bins with constant trajectory number (A), constant N/N_b ratio (B), as a function of the time lag (C), and of simulated motion parameters (D). Shown motion parameters are the diffusion coefficient D for the D model (cyan), the transport velocity V and positional variance k_V for the V model (dark and light green respectively), and the anomalous diffusion coefficient D_α and power exponent α for the A model (magenta and orange, respectively). For panel (D), dark green and magenta dashed lines indicate the errors on estimated V and D_α as a function of varying k_V and α respectively, while plain lines represent the errors on estimated parameters for different input values of the same parameter. Simulated parameters are given in units of default parameters (see main text), except for α (dashed magenta line) where data

points correspond to $\alpha = 0.3, 0.4, 0.5 \dots 0.9$, from left to right. Each data point was obtained after averaging over 20 simulations.

Figure 3: Automated least squares fitting can separate contributions to the JDD of molecule subpopulations experiencing different motion modes. Error on the estimation of the fraction f_D of freely diffusing molecules for composite DD model (A), DV model (B) and DA model (C), with simulated $f_D = 0.5$. Diagrams on the left represent the absolute error on f_D as a function of motion model input parameters (horizontal and vertical axis) as color maps, whose legend is given above each diagram. Plots on the right represent the absolute error on the fraction f_D as a function of the number of bins with constant N (black), with constant $N/N_b = 100$ (light grey), and as a function of the time lag (dark grey). Each data point was obtained after averaging over 20 simulations.

Figure 4: Motion parameters are well measured when estimated subpopulation fractions are accurate. Scatter dot plots showing, for all the motion model and trajectory parameters tested, the relative error on motion parameters measurements (y axis) as a function of the error on the measured freely diffusing subpopulation fraction f_D (x axis) for the DD (A), DV (B) and DA (C) models. Shown motion parameters are the diffusion coefficient of the freely diffusing fraction (cyan, A-C), the (fast) diffusion coefficient of the other freely diffusing fraction for the DD model (dark blue, A), the velocity and positional variance for the DV model (dark and light green respectively, B), and the anomalous diffusion coefficient and power exponent for the DA model (magenta and orange respectively, C). Each data point was obtained after averaging over 20 simulations.

Figure 5: A Bayesian model selection procedure extracts underlying transport mode from simulated JDD. Bar charts showing the output of the Bayesian model selection procedure for various input (simulated) motion models and parameter ranges. Simple and composite input motion modes are represented on panels (A) and (B) respectively. Possible outputs motion modes are: D (cyan), V (light green), A (red), DD (dark blue), DV (dark

green), DA (purple), and undetermined (for simulated JDDs for which all model probabilities provided by the Bayesian procedure are below 75%, grey). Note that special undetermined situations, where the probabilities of V and DV models almost sum to 1 and where the probabilities of A and DA models almost sum to 1, were represented with light to dark green and magenta to purple colour gradients for illustration purposes. For simple input models for which some runs showed a significant probability (larger than 25%) for the corresponding composite model (either larger than 75% - in this case, the run contributes to the occurrence of the composite model – or between 25 and 75% - in this case the run is undetermined), the average fraction of the “correct” input model in the mix was computed and is shown in white. For instance, the $f_V = 0.82$ indicated in the top (green gradient) fraction of the 4th bar chart on panel B means that over the (10%) of the runs for which the procedure yielded an undetermined motion model with models V and DV probabilities summing to almost 1, the average fraction $f_V = 1 - f_D$ of the directly transport population obtained when fitting with the DV model is 0.82. Thus, as expected the contribution of the (input) V motion mode in the procedure output dominates over the D motion mode.

Supplementary Figure legends

Supplementary Figure S1: Measurement of additional motion parameters from automated least squares fitting of the JDD. Relative error on measured motion parameters as a function of simulated motion parameters. Shown measured parameters are the positional variance k_V for the V model (light green), and the anomalous power exponent α for the A model (orange). Light green and orange dashed lines indicate the errors on estimated k_V and α as a function of varying V and D_α respectively, while plain lines represent the errors on estimated parameters for different input values of the same parameter. Simulated parameters are given in units of default parameters (see main text), except for α (plain orange line) where data points correspond to $\alpha = 0.3, 0.4, 0.5 \dots 0.9$, from left to right. Each data point was obtained after averaging over 20 simulations.

Supplementary Figure S2: The accuracy of motion parameter measurement increases with the subpopulation fraction for composite input models. Relative error on measured motion parameters as a function of the input subpopulation fraction for the composite models. Shown motion parameters are the diffusion coefficient of the (slowly) freely diffusing fraction (cyan, 3 lines corresponding to DD, DV and DA input models), the (fast) diffusion coefficient of the other freely diffusing fraction for the DD model (dark blue), the velocity V and positional variance k_V for the DV model (dark and light green respectively, B), and the anomalous diffusion coefficient D_α and power exponent α for the DA model (magenta and orange respectively, C).

Supplementary Figure S3: Limits of the Bayesian model selection procedure and partial improvement with increasing number of trajectories. Bar charts showing the output of the Bayesian model selection procedure for various input (simulated) motion models in parameter ranges for which the least squares fitting is less accurate. Simple and composite input motion modes are represented on panels (A) and (B) respectively. The

colour coding of possible outputs and the simple model fractions in composite and undetermined output models in Panel A are defined as in Figure 5.

References

- [1] K. Jaqaman, D. Loerke, M. Mettlen, H. Kuwata, S. Grinstein, S. L. Schmid et G. Danuser, «Robust single-particle tracking in live-cell time-lapse sequences,» *Nature Methods* 5, pp. 695-702, 2008.
- [2] A. Serge, N. Bertaux, H. Rigneault et D. Marguet, «Dynamic multiple-target tracing to probe spatiotemporal cartography of cell membranes,» *Nat Methods* 5, pp. 687-694, 2008.
- [3] E. Betzig, G. H. Patterson, R. Sougrat, O. W. Lindwasser, S. Olenych, J. S. Bonifacino, J. Lippincott-Schwartz et H. F. Hess, «Imaging Intracellular Fluorescent Proteins at Nanometer Resolution,» *Science* 313, pp. 1642-1645, 2006.
- [4] M. J. Rust, M. Bates et X. Zhuang, «Sub-diffraction-limit imaging by stochastic optical reconstruction microscopy (STORM),» *Nature Methods* 3, pp. 793-796, 2006.
- [5] A. Yildiz, Joseph N. Forkey, S. A. McKinney, T. Ha, Y. E. Goldman et P. R. Selvin, «Myosin V Walks Hand-Over-Hand: Single Fluorophore Imaging with 1.5-nm Localization,» *Science* 300, pp. 2061-2065, 2003.
- [6] N. Shaner, M. Lin, M. Mckeown, P. Steinbach et K. Hazelwood, «Improving the photostability of bright monomeric orange and red fluorescent proteins.,» *Nature Methods* 5, p. 545–551, 2008.
- [7] V. Los, L. Encell, M. Mcdougall, D. Hartzell et N. Karassina, «HaloTag: A Novel Protein Labeling Technology for Cell Imaging and Protein Analysis,» *ACS Chem Biol* 3, p. 373–382, 2008.
- [8] B. Giepmans, S. Adams, M. Ellisman et R. Tsien, «The fluorescent toolbox for assessing protein location and function,» *Science* 312, p. 217–224., 2006.
- [9] D. Janning, M. Igaev, F. Sündermann, J. Brühmann, O. Beutel, J. J. Heinisch, L. Bakota, J. Piehler, W. Junged et a. R. Brandt, «Single-molecule tracking of tau reveals fast kiss-and-hop interaction with microtubules in living neurons,» *Molecular Biology of the Cell* 25, pp. 3541-3551, 2014.
- [10] N. Hoze, D. Nair, E. Hosy, C. Sieben, S. Manley et A. Herrmann, «Heterogeneity of AMPA receptor trafficking and molecular interactions revealed by superresolution analysis of live cell imaging,» *Proc. Nat. Aca. Sci.* 109, p. 17052–17057, 2012.
- [11] A. Constals, A. C. Penn, B. Compans, E. Toulme, A. Phillipat, S. Marais, N. Retailleau, A. -S. Hafner, F. Coussen, E. Hosy et D. Choquet, «Glutamate-Induced AMPA Receptor Desensitization Increases Their Mobility and Modulates Short-Term Plasticity through Unbinding from Stargazin,» *Neuron* 85, pp. 787-803, 2015.
- [12] C. Landes, «Single-Molecule Tracking and Super-Resolution Imaging Shed Light on Cholera

Toxin Transcription Activation,» *Molecular Microbiology* 96, pp. 1-3, 2015.

- [13] M. Ferro, F. Castiglione, C. Punta, L. Melone, W. Panzeri, B. Rossi, F. Trotta et a. A. Mele, «Anomalous diffusion of Ibuprofen in cyclodextrin nanosponge hydrogels: an HRMAS NMR study,» *Beilstein J. Org. Chem.* 10, pp. 2715-2723, 2014.
- [14] A. Baker, A. Saulière, F. Dumas, C. Millot, S. Mazères, A. Lopez et L. Salomé, «Functional membrane diffusion of G-protein coupled receptors.,» *Eur Biophys J* 36, p. 849–860, 2007.
- [15] N. L. Andrews, K. A. Lidke, J. R. Pfeiffer, A. R. Burns, B. S. Wilson, J. M. Oliver et D. S. & Lidke, «Actin restricts FcepsilonRI diffusion and facilitates antigen-induced receptor immobilization,» *Nat Cell Biol* 10, pp. 955-963, 2008.
- [16] I. Izeddin, V. Récamier, L. Bosanac, I. I. Cissé, L. Boudarene, C. Dugast-Darzacq, F. Proux, O. Bénichou, R. Voituriez, O. Bensaude, M. Dahan et X. Darzacq, «Single-molecule tracking in live cells reveals distinct target-search strategies of transcription factors in the nucleus,» *eLife* 3, p. e02230, 2014.
- [17] I. F. Smith, D. Swaminathan, G. D. Dickinson et a. I. Parke, «Single-Molecule Tracking of Inositol Trisphosphate Receptors Reveals Different Motilities and Distributions,» *Biophysical J.* 107, pp. 834-845, 2014.
- [18] M. J. Saxton et K. Jacobson, «SINGLE-PARTICLE TRACKING: Applications to Membrane Dynamics,» *Annual Review of Biophysics and Biomolecular Structure* 26, pp. 373-399, 1997.
- [19] B. Brandenburg et X. Zhuang, «Virus trafficking – learning from single-virus tracking,» *Nature Reviews Microbiology* 5, pp. 197-208, 2007.
- [20] K. Jaqaman, H. Kuwata, N. Touret, R. Collins, W. S. Trimble, G. Danuser et S. Grinstein, «Cytoskeletal control of CD36 diffusion promotes its receptor and signaling function,» *Cell* 146, pp. 593-606, 2011.
- [21] C.-H. Chuang, A. E. Carpenter, B. Fuchsova, T. Johnson, P. de Lanerolle et A. S. Belmont, «Long-range directional movement of an interphase chromosome site.,» *Current Biology* 16, pp. 825-831, 2006.
- [22] T. Cremer et C. Cremer, «Chromosome territories, nuclear architecture and gene regulation in mammalian cells,» *Nature Reviews Genetics* 2, pp. 293-301, 2001.
- [23] M. Mori, N. Monnier, N. Daigle, M. Bathe, J. Ellenberg et P. Lénárt, «Intracellular transport by an anchored homogeneously contracting F-actin meshwork.,» *Current Biology* 21, pp. 606-11, 2001.
- [24] T. S. Kitajima, M. Ohsugi et J. Ellenberg, «Complete Kinetochore Tracking Reveals Error-Prone Homologous Chromosome Biorientation in Mammalian Oocytes,» *Cell* 146, pp. 568-581, 2011.

- [25] M. Gardner, C. Pearson, B. Sprague, T. Zarzar, K. Bloom, E. Salmon et D. Odde, «Tension-dependent regulation of microtubule dynamics at kinetochores can explain metaphase congression in yeast,» *Mol Biol Cell* 8, pp. 3764-75, 2005.
- [26] M. Ehrlich, W. Boll, A. v. Oijen, R. Hariharan, K. Chandran, M. L. Nibert et T. Kirchhausen, «Endocytosis by Random Initiation and Stabilization of Clathrin-Coated Pits,» *Cell* 118, pp. 591-605, 2004.
- [27] L. Turner, W. S. Ryu et H. C. Berg, «Real-Time Imaging of Fluorescent Flagellar Filaments,» *Journal of Bacteriology* 182, pp. 2793-2801, 2000.
- [28] J. P. Siebrasse, R. Veith, A. Dobay, H. Leonhardt, B. Daneholt et a. U. Kubitscheck, «Discontinuous movement of mRNP particles in nucleoplasmic regions devoid of chromatin,» *Proc. Nat. Aca. Sci. USA* 105, p. 20291–20296, 2008.
- [29] M. F. Serag, M. Abadi et S. Habuchi, «Single-molecule diffusion and conformational dynamics by spatial integration of temporal fluctuations,» *Nature Communications* 5, p. DOI: 10.1038, 2014.
- [30] K. Jaqaman et G. Danuser, «Linking data to models: data regression,» *Nat. Rev. Mol. Cell Biol.* 7, pp. 813-819, 2006.
- [31] H. Qian et S. C. Kou, «Statistics and Related Topics in Single-Molecule Biophysics,» *Annu Rev Stat Appl.*, pp. 465-492, 2014.
- [32] X. Michalet, «Mean square displacement analysis of single-particle trajectories with localization error: Brownian motion in an isotropic medium,» *Phys. Rev. E* 82, p. 041914, 2010.
- [33] I. Sbalzarini et P. Koumoutsakos, «Feature point tracking and trajectory analysis for video imaging in cell biology,» *J Struct Biol* 151, pp. 182-195, 2005.
- [34] I. Izeddin, J. Boulanger, V. Racine, C. Specht, A. Kechkar, D. Nair, A. Triller, D. Choquet, M. Dahan et a. J. Sibarita, «Wavelet analysis for single molecule localization microscopy,» *OPTICS EXPRESS* 20, pp. 2081-2095, 2012.
- [35] K. C. Robben, K.-H. Tran-Ba, T. Ito et a. D. A. Higgins, «Trajectory-Profile-Guided Single Molecule Tracking for Assignment of One-Dimensional Diffusion Trajectories,» *Anal. Chem.* 86, p. 10820–10827, 2014.
- [36] M. B. Smith, E. Karatekin, A. Gohlke, H. Mizuno et a. D. Vavylonis, «Interactive, Computer-Assisted Tracking of Speckle Trajectories in Fluorescence Microscopy: Application to Actin Polymerization and Membrane Fusion,» *Biophysical J.* 101, p. 1794–1804, 2011.
- [37] A. W. Harrison, D. A. Kenwright, T. A. Waigh, P. G. Woodman et a. V. J. Allan, «Modes of correlated angular motion in live cells across three distinct time scales,» *Phys. Biol.* 10, p. 036002, 2013.

- [38] D. A. Kenwright, A. W. Harrison, T. A. Waigh, P. G. Woodman et a. V. J. Allan, «First-passage-probability analysis of active transport in live cells,» *Physical Review E* 86, p. 031910, 2012.
- [39] B. M. Regner, D. Vucin, C. Domnisoru, T. M. Bartol, M. W. Hetzer, D. M. Tartakovsky et a. T. J. Sejnowski, «Anomalous Diffusion of Single Particles in Cytoplasm,» *BiophysicalJ.* 104, p. 1652–1660, 2013.
- [40] B. Shuang, C. P. Byers, L. Kisley, L.-Y. Wang, J. Zhao, H. Morimura, S. Link et a. C. F. Landes, «Improved Analysis for Determining Diffusion Coefficients from Short Single-Molecule Trajectories with Photoblinking,» *Langmuir* 29, p. 228–234, 2013.
- [41] V. Tejedor, O. Benichou, R. Voituriez, R. Jungmann, F. Simmel, C. Selhuber-Unkel, L. B. Oddershede et a. R. Metzler, «Quantitative Analysis of Single Particle Trajectories: Mean Maximal Excursion Method,» *BiophysicalJ.* 98, p. 1364–1372, 2010.
- [42] S. Huet, E. Karatekin, V. S. Tran, I. Fanget, S. Cribier et a. J.-P. Henry, «Analysis of Transient Behavior in Complex Trajectories: Application to Secretory Vesicle Dynamics,» *BiophysicalJ.* 91, p. 3542–3559, 2006.
- [43] D. Arcizet, B. Meier, E. Sackmann, J. O. Radler et D. Heinrich, «Temporal Analysis of Active and Passive Transport in Living Cells,» *Physical Review Letters* 101, p. 248103, 2008.
- [44] H. Qian et M. E. E. Sheetz, «Single particle tracking. Analysis of diffusion and flow in two-dimensional systems,» *Biophys J* 60, pp. 910-921, 1991.
- [45] A. G. Cherstvyva et R. Metzler, «Population splitting, trapping, and non-ergodicity in heterogeneous diffusion processes,» *Phys.Chem. Chem. Phys.* 15, p. 20220, 2013.
- [46] E. Sarmiento-Gomez, I. Santamaría-Holek et a. R. Castillo, «Mean-Square Displacement of Particles in Slightly Interconnected Polymer Networks,» *J. Phys. Chem. B* 118, pp. 1146-1158, 2014.
- [47] H. Berry et H. Chaté, «Anomalous diffusion due to hindering by mobile obstacles undergoing Brownian motion or Orstein-Uhlenbeck processes,» *Physical Review E* 89, p. 022708, 2014.
- [48] M. R. Shaebani, Z. Sadjadi, I. M. Sokolov, H. Rieger et a. L. Santen, «Anomalous Diffusion of Self-Propelled Particles in Directed Random Environments,» *arXiv:1407.0810v2*, 2014.
- [49] M. Saxton, «Single-particle tracking: connecting the dots.,» *Nature Methods* 5, p. 671–672 , 2008.
- [50] L. Barak et W. Webb, «Diffusion of low density lipoprotein-receptor complex on human fibroblasts.,» *J Cell Biol* 95, pp. 846-852, 1982.
- [51] D. Alcor, G. Gouzer et A. Triller, «Single-particle tracking methods for the study of membrane receptors dynamics.,» *Eur J Neurosci* 30, pp. 987-997, 2009.

- [52] M. Goulian et S. Simon, «Tracking single proteins within cells.» *Biophys J* 79, pp. 2188-2198, 2000.
- [53] A. Bruckbauer, P. James, D. Zhou, J. W. Yoon, D. Excell, Y. Korchev et D. Klenerman, «Nanopipette delivery of individual molecules to cellular compartments for single-molecule fluorescence tracking.» *Biophys J* 93, pp. 3120-3131, 2007.
- [54] M. Jose, S. Tollis, D. Nair, R. Mitteau, C. Velours, A. Massoni-Laporte, A. Royou, J.-B. Sibarita et a. D. McCusker, «A quantitative imaging-based screen reveals the exocyst as a network hub connecting endo- and exocytosis.» *Molecular Biology of the Cell*, pp. E14-11-1527, 2015.
- [55] O. Rossier, V. Oceau, J.-B. Sibarita, C. Leduc, B. Tessier, D. Nair, V. Gatterdam, O. Destaing, C. Albigès-Rizo, R. Tampé, L. Cognet, D. Choquet, B. Lounis et a. G. Giannone, «Integrins B1 and B3 exhibit distinct dynamic nanoscale organizations inside focal adhesions.» *Nature Cell Biology* 14, pp. 1057-1069, 2012.
- [56] R. Metzler et J. Klafter, «THE RANDOM WALK: S GUIDE TO ANOMALOUS DIFFUSION: A FRACTIONAL DYNAMICS APPROACH.» *Physics Reports* 339, pp. 1-77, 2000.
- [57] M. Otten, A. Nandi, D. Arcizet, M. Gorelashvili, B. Lindner et a. D. Heinrich, «Local Motion Analysis Reveals Impact of the Dynamic Cytoskeleton on Intracellular Subdiffusion.» *Biophysical J.* 102, p. 758-767, 2012.
- [58] M. Saxton, «Single-particle tracking: the distribution of diffusion coefficients.» *Biophys J* 72, pp. 1744-1753, 1997.
- [59] B. Flier, M. Baier, J. Huber, K. Müllen, S. Mecking, A. Zumbusch et D. Wöll, «Single molecule fluorescence microscopy investigations on heterogeneity of translational diffusion in thin polymer films.» *Phys Chem Chem Phys* 13, pp. 1770-1775, 2011.
- [60] E. Kepten, A. Weron, G. Sikora, K. Burnecki et Y. Garini, «Guidelines for the Fitting of Anomalous Diffusion Mean Square Displacement Graphs from Single Particle Tracking Experiments.» *PLoS one* 10, p. e0117722, 2015.
- [61] R. Metzler, V. Tejedor et J.-H. Jeon, ANALYSIS OF SINGLE PARTICLE TRAJECTORIES: FROM NORMAL TO ANOMALOUS DIFFUSION, 2009: 1315-1331, Acta Physica Polonica B 40.
- [62] I. Bronstein, Y. Israel, E. Kepten, S. Mai, Y. Shav-Tal, E. Barkai et a. Y. Garini, «Transient Anomalous Diffusion of Telomeres in the Nucleus of Mammalian Cells.» *Physical Review Letters* 103, p. 018102, 2009.
- [63] F. B. Robin, W. M. McFadden, B. Yao et a. E. M. Munro, «High-density single-molecule analysis of cell surface dynamics in *C. elegans* embryos.» *Nature Methods* 11, p. 677-682, 2014.
- [64] H. Zhan, R. Stanciauskas, C. Stigloher, K. K. Dizon, M. Jospin, J.-L. Bessereau et & F. Pinaud, «In vivo single-molecule imaging identifies altered dynamics of calcium channels in dystrophin-

- mutant *C. elegans*,» *Nature Communications* 5, p. 4974, 2014.
- [65] C. Anderson, G. Georgiou, I. Morrison, G. Stevenson et R. Cherry, «Tracking of cell surface receptors by fluorescence digital imaging microscopy using a charge-coupled device camera. Low-density lipoprotein and influenza virus receptor mobility at 4 degrees C.,» *J Cell Sci* 101, pp. 415-425, 1992.
- [66] G. Schütz, H. Schindler et T. Schmidt, «Single-molecule microscopy on model membranes reveals anomalous diffusion.,» *Biophys J* 73, pp. 1073-1080, 1997.
- [67] D. Grünwald, R. M. Martin, V. Buschmann, D. P. Bazett-Jones, H. Leonhardt, U. Kubitscheck et M. C. & Cardoso, «Probing intranuclear environments at the single-molecule level,» *Biophys J* 94, pp. 2847-2858, 2008.
- [68] J. P. Siebrasse, R. Veith, A. Dobay, H. Leonhardt, B. Daneholt et U. & Kubitscheck, «Discontinuous movement of mRNP particles in nucleoplasmic regions devoid of chromatin.,» *Proc Natl Acad Sci U S A* 105, pp. 20291-20296, 2008.
- [69] L. Weimann, K. A. Ganzinger, J. McColl, K. L. Irvine et S. J. Davis, «A Quantitative Comparison of Single-Dye Tracking,» *PLoS one* 8, p. e64287, 2013.
- [70] S. Wieser, M. Moertelmaier, E. Fuertbauer, H. Stockinger et G. Schütz, «(Un)confined diffusion of CD59 in the plasma membrane determined by high-resolution single molecule microscopy.,» *Biophys J* 92, pp. 3719-3728, 2007.
- [71] S. Wieser, M. Axmann et G. Schütz, «Versatile analysis of single-molecule tracking data by comprehensive testing against Monte Carlo simulations.,» *Biophys J* 95, pp. 5988-6001, 2008.
- [72] A. Sonnleitner, G. Schütz et T. Schmidt, «Free Brownian Motion of Individual Lipid Molecules in Biomembranes.,» *Biophys J* 77, pp. 2638-2642, 1999.
- [73] T. Bickel, «A note on confined diffusion,» *arXiv:cond-mat/0604133v2*, 2006.
- [74] A. Kusumi, Y. Sako et M. Yamamoto, «Confined lateral diffusion of membrane receptors as studied by single particle tracking (nanovid microscopy). Effects of calcium-induced differentiation in cultured epithelial cells,» *Biophys. J.*, 65, pp. 2021-2040, 1993.
- [75] D. P. T. Buckley, «Model selection and model averaging in phylogenetics: advantages of Akaike Information Criterion and Bayesian approaches over likelihood ratio tests,» *Syst. Biol.*, 53, pp. 793-808, 2004.
- [76] N. Friedman, «Inferring cellular networks using probabilistic graphical models,» *Science* 303, pp. 797-805, 2004.
- [77] N. Monnier, S.-M. Guo, M. Mori, J. He, P. Lénárt et M. Bathe, «Bayesian Approach to MSD-Based Analysis of Particle Motion in Live Cells,» *Biophysical J.* 103, p. 616–626, 2012.

- [78] D. Sivia et J. Skilling, *Data Analysis: A Bayesian Tutorial*, Oxford: Oxford University Press, 2006.
- [79] A. Raftery, «Bayesian model selection in social research,» *Sociol. Methodol.*, *25*, pp. 111-163, 1995.
- [80] B. Carlin et T. Louis, *Bayesian Methods for Data Analysis*, Boca Raton: CRC Press, 2009.
- [81] M. Beaumont et B. Rannala, «The Bayesian revolution in genetics,» *Nat. Rev. Genet.*, *5*, pp. 251-261, 2004.
- [82] K. Sachs, O. Perez, D. Pe'er, D. A. Lauffenburger et G. P. Nolan, «Causal protein-signaling networks derived from multiparameter single-cell data,» *Science*, *308*, pp. 523-529, 2005.
- [83] J. E. Bronson, J. Fei, J. M. J. Hofman, R. L. Gonzalez et a. C. H. Wiggins, «Learning rates and states from biophysical time series: a Bayesian approach to model selection and single-molecule FRET data,» *Biophys. J.*, *97*, pp. 3196-3205, 2009.
- [84] J. He, S. Guo et M. Bathe, «Bayesian approach to the analysis of fluorescence correlation spectroscopy data I: theory,» *Anal. Chem.*, *84*, pp. 3871-3879, 2012.
- [85] S.-M. Guo, J. He, N. Monnier, G. Sun, T. Wohland et M. Bathe, «Bayesian approach to the analysis of fluorescence correlation spectroscopy data II: application to simulated and in vitro data,» *Anal. Chem.*, *84*, pp. 3880-3888, 2012.
- [86] D. Posada et T. Buckley, «Model selection and model averaging in phylogenetics: advantages of Akaike Information Criterion and Bayesian approaches over likelihood ratio tests,» *Syst. Biol.*, *53*, pp. 793-808, 2004.
- [87] S. Hasnain, C. L. McClendon, M. T. Hsu et M. P. Jacobson, «A New Coarse-Grained Model for E. coli Cytoplasm: Accurate Calculation of the Diffusion Coefficient of Proteins and Observation of Anomalous Diffusion,» *PLoS one*, p. e106466, 2014.
- [88] E. R. Weeks, J. Urbach et H. L. Swinney, «Anomalous diffusion in asymmetric random walks with a quasi-geostrophic flow example,» *Physica C* *97*, pp. 291-310, 1996.
- [89] O. Chepizhko et a. F. Peruani, «Diffusion, subdiffusion, and trapping of active particles in heterogeneous media,» *arXiv:1310.0830v1*, 2013.
- [90] A. Kilbas, T. Pierantozzi, J. Trujillo et L. Vazquez, «On the solution of fractional evolution,» *J Phys A: Math Gen* *37*, pp. 3271-3282, 2004.
- [91] A. Kahana, G. Kenan, M. Feingold, M. Elbaum et a. R. Granek, «Active transport on disordered microtubule networks: The generalized random velocity model,» *PHYSICAL REVIEW E* *78*, p. 051912, 2008.
- [92] D. Del-Castillo-Negrete, B. Carreras et V. Lynch, «Front dynamics in reaction-diffusion systems,»

Physical Review Letters 91, p. 018302, 2003.

- [93] J. Klafter et I. M. Sokolov, «Anomalous diffusion spreads its wings,» *Physics World*, August 2005.
- [94] M. Y. Ali, H. Lu, C. S. Bookwalter, D. M. Warshaw et K. M. Trybus, «Myosin V and Kinesin act as tethers to enhance each others' processivity.,» *Proc. Natl. Acad. Sci. U.S.A.* 105, pp. 4691-4696, 2008.
- [95] D. Oh, Y. Yu, H. Lee, B. L. Wanner et a. K. Ritchie, «Dynamics of the Serine Chemoreceptor in the Escherichia coli Inner Membrane: A High-Speed Single-Molecule Tracking Study,» *Biophysical J.* 106, pp. 145-153, 2014.
- [96] L. Stixová, E. Bártová, P. Matula, O. Daněk, S. Legartová et S. Kozubek, «Heterogeneity in the kinetics of nuclear proteins and trajectories of substructures associated with heterochromatin,» *Epigenetics & Chromatin* 4, pp. 5-21, 2011.
- [97] P. J. Bosch, I. R. C. Jr., M. H. Sonntag, J. Ibach, L. Brunsveld, J. S. Kanger et V. Subramaniam, «Evaluation of Fluorophores to Label SNAP-Tag Fused Proteins for Multicolor Single-Molecule Tracking Microscopy in Live Cells,» *Biophys. J.* 107, pp. 803-814, 2014.
- [98] M. Fernandez-Suarez et A. Y. Ting, «Fluorescent probes for super-resolution imaging in live cells,» *Nat. Rev.* 9, pp. 929-943, 2008.
- [99] D. S. Grebenkov, M. Vahabi, E. Bertseva, L. Forro et S. Jeney, «Evidence of hydrodynamic and subdiffusive motion of tracers in a viscoelastic medium,» *arXiv:1305.3387*, 2013.
- [100] K. H. T. N. C. R. T. W. D. G. G. S. Jaqaman K, «Cytoskeletal control of CD36 diffusion promotes its receptor and signaling function.,» *Cell* 146, pp. 593-606, 2011.

Materials and Methods

Characterizing single molecule motion using the Jump Distance Distribution

The method described in this article was developed to analyze a set of N individual planar trajectories, or fraction of trajectories, labelled with the index $j = 1..N$. All trajectories are assumed to have an identical duration $\tau = M\delta t$ and comprise of $M + 1$ points of planar Cartesian coordinates x_j^p and y_j^p , $p = 1..M + 1$; δt is the time step between two consecutive measurements of single molecules' positions. For each trajectory, the jump distance, e.g. the geometrical distance between its first and last points, is defined by:

$$l_j = \sqrt{(x_j^{M+1} - x_j^1)^2 + (y_j^{M+1} - y_j^1)^2} .$$

The experimental jump distance distribution (JDD) is defined by classifying the N jump distances in ordered bins of fixed size (see Figure 1A). In this work, we have chosen to control the number of bins, denoted N_b . Hence, the bin size is $\delta r = \frac{\max(l_j)}{N_b}$. By definition, a trajectory is added to the i^{th} bin if and only if $r_i - \delta r/2 < l_j \leq r_i + \delta r/2$ where $r_i = (i - 1/2)\delta r$ is the median point of the bin. The distribution is therefore defined by the set of integer numbers $\{N_i, i = 1..N_b, \sum_{i=1}^{N_b} N_i = N\}$ corresponding to the number of trajectories in each bin for the analyzed dataset.

For the simple models D, V and A considered in this study, closed form formulas have been derived mathematically in the past for the theoretical jump distance probability distribution (JDP) [56,73,90-92]. The corresponding jump distance distributions for the simple models $\{\tilde{N}_i^{D,V,A}, i = 1..N_b\}$ are easily obtained by multiplying the JDPs by the number of molecules, and we get respectively:

$$\tilde{N}_i^D = N \delta r \frac{r_i}{2D\tau} e^{-\frac{r_i^2}{4D\tau}}$$

$$\tilde{N}_i^V = N \delta r \frac{r_i}{Mk_V} e^{-\frac{r_i^2 + V^2 \tau^2}{2Mk_V}} I_0\left(\frac{r_i V \tau}{k_V}\right),$$

where the averaging over the directed tracks (assumed to be distributed isotropically with respect to the plane of the plasma membrane) has been performed, Mk_V is the variance of the molecule position over the M supposedly independent steps of a trajectory with $M + 1$ points, and I_0 is the modified Bessel function of the first kind. \tilde{N}_i^A is defined by an inverse Laplace transform:

$$\tilde{N}_i^A = N \delta r \frac{r_i}{D_\alpha} \int_{-i\gamma - \infty}^{-i\gamma + \infty} e^{ip\tau} \frac{(ip)^{\alpha-1}}{2\pi} K_0\left(\frac{r_i}{\sqrt{D_\alpha}} (ip)^{\alpha/2}\right) dp,$$

where K_0 is the modified Bessel function of the second kind, and the cutoff γ is small. Unless otherwise specified, for numerical evaluations of \tilde{N}_i^A the cutoff γ was set to the working precision of our computations, and the integral boundaries were set to ± 300 for $\alpha \geq 0.5$, and $(300)^{0.5/\alpha}$ for $\alpha < 0.5$. Indeed, the slow decrease of the Bessel function with p for small values of α makes it necessary to integrate over a broader range to get a good estimate of the inverse Laplace transform.

The theoretical JDD for models encompassing two subpopulations of molecules experiencing different motion modes are readily obtained:

$$\tilde{N}_i^{DD} = f_D \tilde{N}_i^D + (1 - f_D) \tilde{N}_i^{D2},$$

$$\tilde{N}_i^{DV} = f_D \tilde{N}_i^D + (1 - f_D) \tilde{N}_i^V,$$

$$\tilde{N}_i^{DA} = f_D \tilde{N}_i^D + (1 - f_D) \tilde{N}_i^A,$$

where f_D denotes the fraction of molecules diffusing freely. In the following, we show that model optimization, e.g. the search for model parameters that correspond to the maximum likelihood of observing the actual experimental data given a putative motion model X , is obtained through the minimization of the generalized squared error $\sum_{i=1}^{N_b} w_i (\tilde{N}_i^X - N_i)^2$ with some specific weights w_i that we determine.

Bayesian approach for model selection on JDD data

For K competing models M_k (here, $K = 6$, $k = 1..K$), and a set of observed data $\{N_i\}$, the probability of each model to be the actual underlying motion mode that produced $\{N_i\}$ is given by the Bayes theorem [77]:

$$P(M_k|\{N_i\}) = \frac{P(\{N_i\}|M_k)P(M_k)}{\sum_{k=1}^K P(\{N_i\}|M_k)P(M_k)}$$

With no a priori knowledge on the underlying motion model, which is generally the case when SMT analysis begins, all the models considered are a priori equiprobable. Hence, $P(M_k) = 1/K$ and this remains the case as long as the user includes all plausible underlying motion models. The following approach remains valid if one wants to add information on the motion mode to the analysis by specifying non equal priori probabilities $P(M_k)$, e.g. by “preferring” such or such model, for instance based on the qualitative visual observation of the JDD.

As a consequence, model probabilities reduce to:

$$P(M_k|\{N_i\}) = \frac{P(\{N_i\}|M_k)}{\sum_{k=1}^K P(\{N_i\}|M_k)}$$

The marginal probability $P(\{N_i\}|M_k)$ is obtained by expanding over the model parameter space:

$$P(\{N_i\}|M_k) = \int P(\{N_i\}|M_k, \beta_k) P(\beta_k|M_k) d\beta_k$$

where the (multiple) integration is performed over the entire range of values of model parameters β_k . Here, β_k denotes the entire set of model parameters. $P(\beta_k|M_k)$ will be specified later in the following.

To calculate $P(\{N_i\}|M_k, \beta_k)$, we assume that the jump distances along different trajectories are independent random variables. Given a motion model M_k with its parameter set β_k , for a

single trajectory of duration τ the probability p_i that the jump distance falls in the i^{th} bin is, by definition, deduced from the JDD of the corresponding model:

$p_i = \frac{\tilde{N}_i^{M_k}}{N}$. For instance, if the model M_k is the free diffusion with the single parameter β_k

being the diffusion coefficient D , $p_i = \frac{\tilde{N}_i^D}{N} = \delta r \frac{r_i}{2D\tau} e^{-\frac{r_i^2}{4D\tau}}$. Since the jump distances of different trajectories are assumed to be independent variables, the probability $P(\{N_i\}|M_k, \beta_k)$ satisfies a multinomial distribution:

$$P(\{N_i\}|M_k, \beta_k) = \frac{N!}{N_1! N_2! \dots N_{N_b}!} p_1^{N_1} p_2^{N_2} \dots p_{N_b}^{N_{N_b}}$$

with the usual constraint $\sum_{i=1}^{N_b} N_i = N$, and where the probabilities p_i depend on the model and its parameters. Although exact, this expression is untractable in numerical computations, so we proceeded to approximate $P(\{N_i\}|M_k, \beta_k)$ using the Laplace's saddle-point approximation.

Starting with the Stirling formula for large integers (larger than a few units), $N! \sim \sqrt{2\pi N} \left(\frac{N}{e}\right)^N$,

with $N^N = e^{N \ln N}$ and using the renormalized bin populations $y_i = N_i/N$ we get:

$$P(\{N_i\}|M_k, \beta_k) \sim \frac{\sqrt{2\pi N}}{\prod_i \sqrt{2\pi N y_i}} e^{N \ln N - \sum_i N_i \ln N_i + \sum_i N_i \ln p_i} = \frac{\sqrt{2\pi N}}{\prod_i \sqrt{2\pi N y_i}} e^{-N(\sum_i [y_i \ln y_i - y_i \ln p_i])} =$$

$$e^{-N\left(\sum_i [y_i \ln y_i - y_i \ln p_i] - \frac{\ln(\sqrt{2\pi N})}{N} + \frac{\sum_i \ln \sqrt{2\pi N y_i}}{N}\right)}$$

where we used the fact that $\sum_i y_i = 1$.

In the latter expression, y_i, p_i , are of order of unity, $\frac{\ln(\sqrt{2\pi N})}{N}$ and $\frac{\sum_i \ln \sqrt{2\pi N y_i}}{N}$ are of respective orders $\frac{\ln(N)}{N}$ and $\frac{N_b \ln(N)}{N}$, both $\ll 1$ provided that the number of bins is small compared to the number of trajectories, N , which is a large number (typically, several thousands). Therefore, $P(\{N_i\}|M_k, \beta_k)$ is maximal for $F(\{y_i\}) = \sum_i [y_i \ln y_i - y_i \ln p_i]$ minimal and decreases very fast, owing to the factor e^{-N} , as soon as $F(\{y_i\})$ deviates from its minimal value. As a

consequence it is sufficient to calculate $P(\{N_i\}|M_k, \beta_k)$ for configurations $\{y_i\}$ such that $F(\{y_i\})$ is close to its minimum, given an underlying model and its parameters that fix the jump distance probabilities $\{p_i\}$. For other configurations, $P(\{N_i\}|M_k, \beta_k) \sim 0$. The minimization of $F(\{y_i\})$ with respect to $\{y_i\}$ under the constraint $G(\{y_i\}) = \sum_i y_i - 1 = 0$ is achieved if $\vec{\nabla}F = \varphi \vec{\nabla}G$ where φ is a Lagrange multiplier, which yields $\forall i \ 1 + \ln y_i - \ln p_i = \varphi$ from which we derive $y_i = p_i e^{\varphi-1}$. The normalization condition $\sum_i y_i = \sum_i p_i = 1$ imposes $\varphi = 1$ and finally we get $y_i = p_i$, or in vector formulation $\vec{y} = \vec{p}$.

$F(\{y_i\})$ is then expanded around the minimum:

$$F(\vec{y}) = F(\vec{p}) + \vec{\nabla}F \cdot (\vec{y} - \vec{p}) + \frac{1}{2} (\vec{y} - \vec{p})^T \Delta F (\vec{y} - \vec{p}),$$

where the gradient $\vec{\nabla}F$ and the Hessian matrix ΔF are evaluated at the minimum $\vec{y} = \vec{p}$. $F(\vec{p}) = 0$, $\vec{\nabla}F \cdot (\vec{y} - \vec{p}) = \sum_i (1 + \ln p_i - \ln p_i) (y_i - p_i) = \sum_i y_i - \sum_i p_i = 0$, while the Hessian matrix is diagonal and $\Delta F_{ii} = \frac{1}{p_i}$.

Finally, we obtain:

$$P(\{N_i\}|M_k, \beta_k) \sim \frac{\sqrt{2\pi N}}{\prod_i \sqrt{2\pi N p_i}} e^{-\frac{N}{2} \sum_{i=1}^{N_b} \frac{(y_i - p_i)^2}{p_i}},$$

with $y_i = N_i/N$ represents the experimental data, and the reference probabilities p_i depend on the model M_k and its parameter(s) β_k .

Minimization of the argument in the exponential function of the previous expression yields the parameters that maximize the likelihood $P(\{N_i\}|M_k, \beta_k)|_{max} = P(\{N_i\}|M_k, \beta_k^0)$ to observe the experimental JDD given the putative model M_k (the ‘‘measured’’ parameters, β_k^0 , see main text). Simulations have allowed us to estimate the accuracy $\delta\beta_k$ to which the motion model parameters could be measured. Following the procedure described in [77], we defined the parameter range $[\beta_k^{min}, \beta_k^{max}]$ over which the probability $P(\{N_i\}|M_k, \beta_k)$ is integrated as a

symmetric interval centred in β_k^0 , the maximum likelihood estimation of β_k , and with a width proportional to the uncertainty $\delta\beta_k$ on parameter measurement. This procedure provides an opportunity to penalize models with too many parameters, and also models for which parameters may be measured inaccurately.

Monte Carlo simulation of single molecules trajectories

Stochastic two-dimensional single vesicle trajectories were simulated using random walks corresponding to the different motion models considered in this study.

Pure diffusion (model “D”) was implemented by generating random, Gaussian distributed independent moves (steps) in the two directions of space at every time point (with a time increment corresponding to the observation time, e.g. $\delta t = 20ms$), using the *randn* function in Matlab. The only parameter of the model, e.g. the diffusion coefficient D , is related to the variance $\langle \Delta x^2 \rangle = \langle \Delta y^2 \rangle$ of the space steps by $\langle \Delta x^2 \rangle = 2D\delta t$.

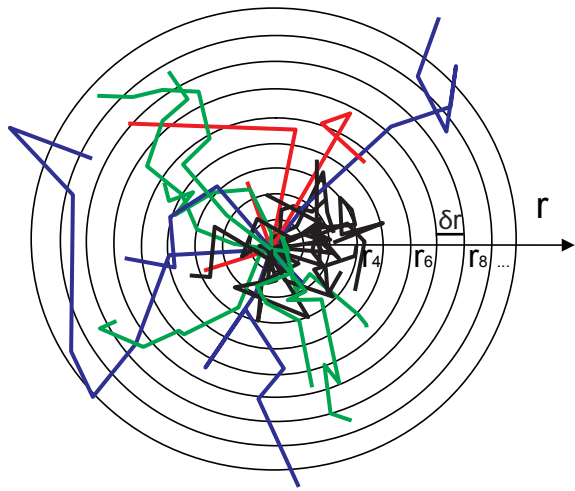
Directed motion (model “V”) was implemented by generating, for each trajectory, random displacements which include: a directed component $\delta x_1 = V\delta t \cos \theta$, $\delta y_1 = V\delta t \sin \theta$ which corresponds to a vesicle being transported at the velocity V along an actin track of random orientation θ during the time increment δt ; a “noise” component, to account for fluctuations of the vesicle position around the actin track, modelled by Gaussian distributed (*randn*) additional displacements in the two directions of space with variance $\langle \Delta x^2 \rangle = \langle \Delta y^2 \rangle \geq k_V$. Typically, k_V scales as $2D\delta t$, where D is the apparent diffusion coefficient of the Brownian motion around the “mean” directed motion of vesicles along the tracks. This model is therefore described by 2 parameters, V and k_V .

Anomalous diffusion (motion model “A”) was implemented using a continuous time random walk with waiting times (CTRW, [56,93]). Similar to the pure diffusion process, random space steps were generated from a Gaussian distribution of variance $\langle \Delta x^2 \rangle = \langle \Delta y^2 \rangle$. However, each move was being attributed a random time, sampled from a long-tailed distribution,

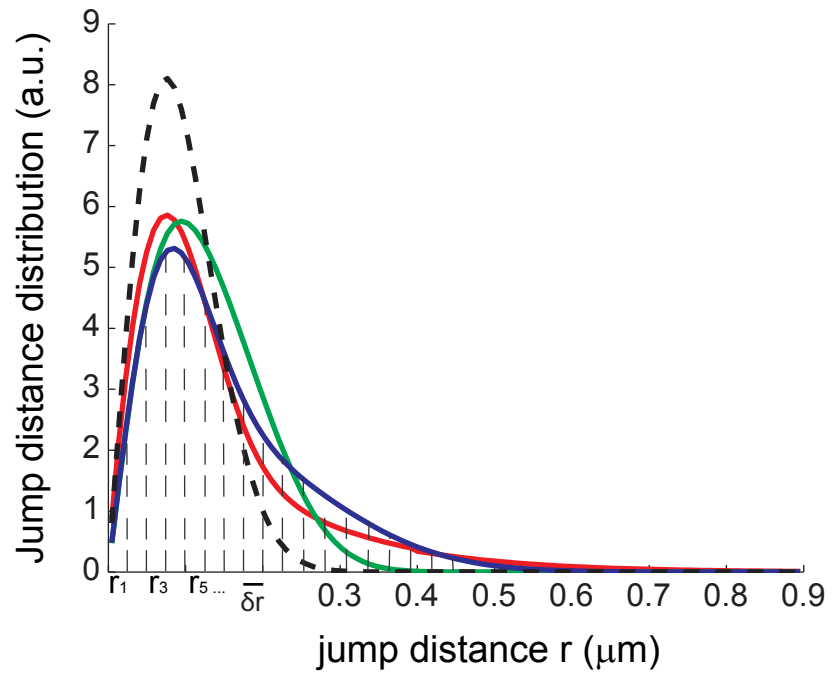
which do not necessarily correspond to the observation times spaced by δt . In this purpose, we calculated the cumulative distribution of waiting times (probability that the vesicle moves before a certain date t), which varies from 0 at $t = 0$ to 1 at $t = \infty$. Then, we generated a random number between 0 and 1, and by identifying this number to the cumulative distribution we obtained the date of the next move. The position of the vesicle at the observation times was inferred from its position immediately before the next move. For the distribution of waiting times, we chose a distribution with a Pareto-like tail (decrease as $(1/t)^{\alpha+1}$ at large times $\gg \delta t'$), and a linear increase with time at short times $t < \delta t'$, with $\delta t' = \delta t/2000 = 0.01\text{ms}$, for regularization. This distribution yields anomalous diffusion at large time lags, with an anomalous exponent α and an effective diffusion coefficient $D_\alpha = \langle \Delta x, y^2 \rangle / 2(\delta t')^\alpha$ [56,93]. Composite models DD, DV, DA were implemented by generating a fraction f_D of free diffusion trajectories, and a fraction $1 - f_D$ of trajectories of the D, V or A type respectively.

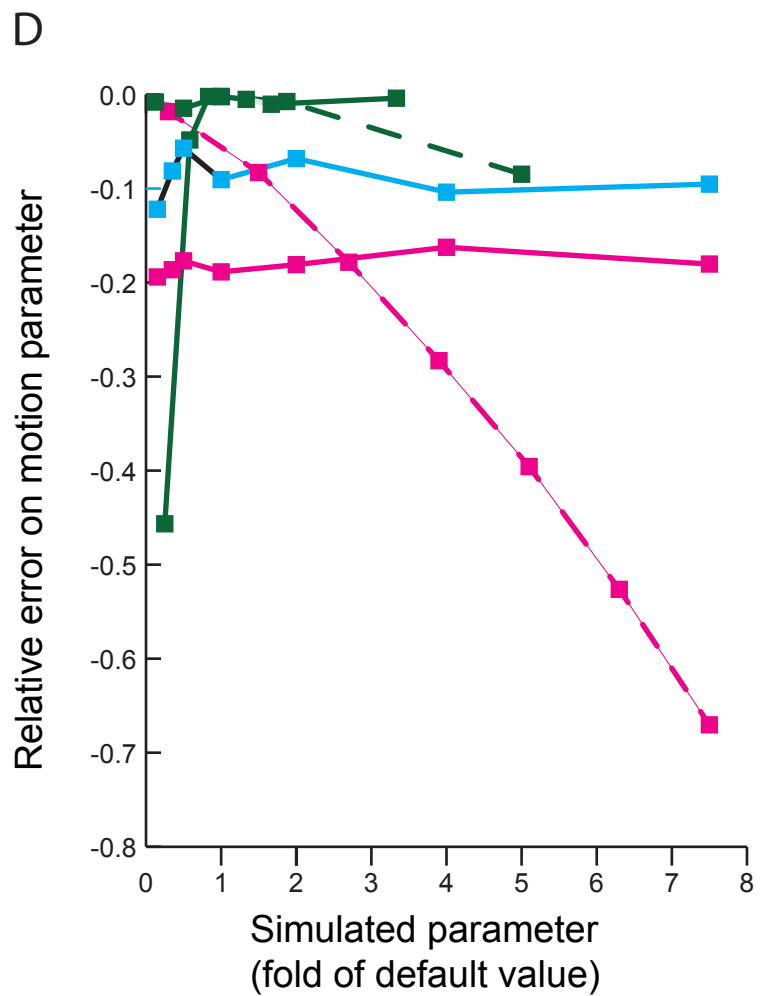
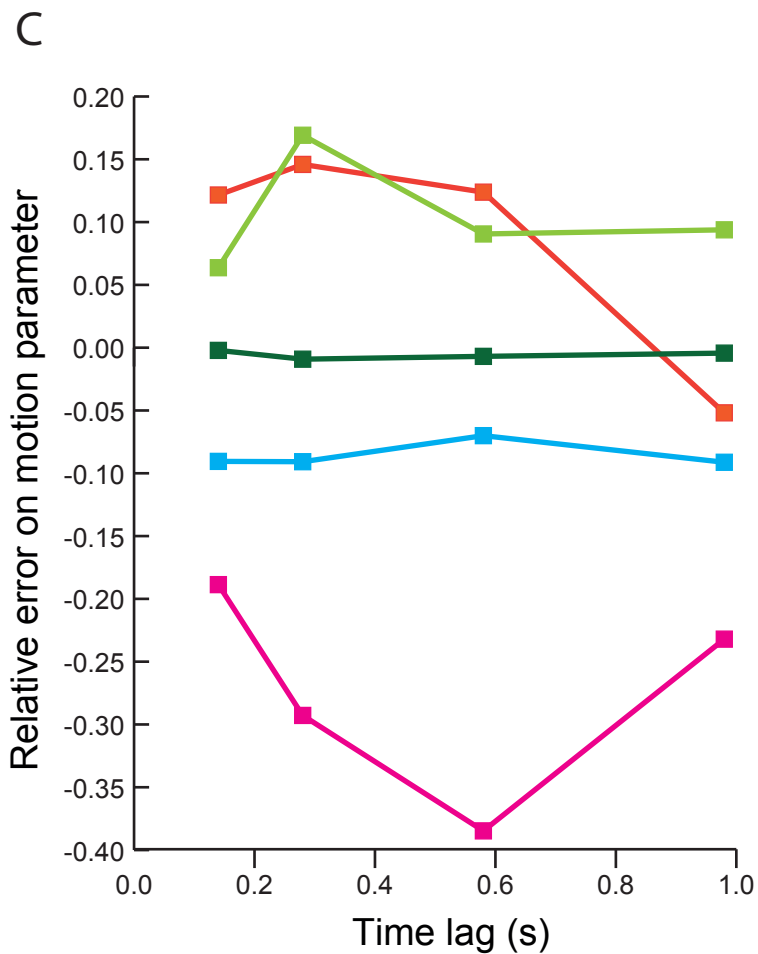
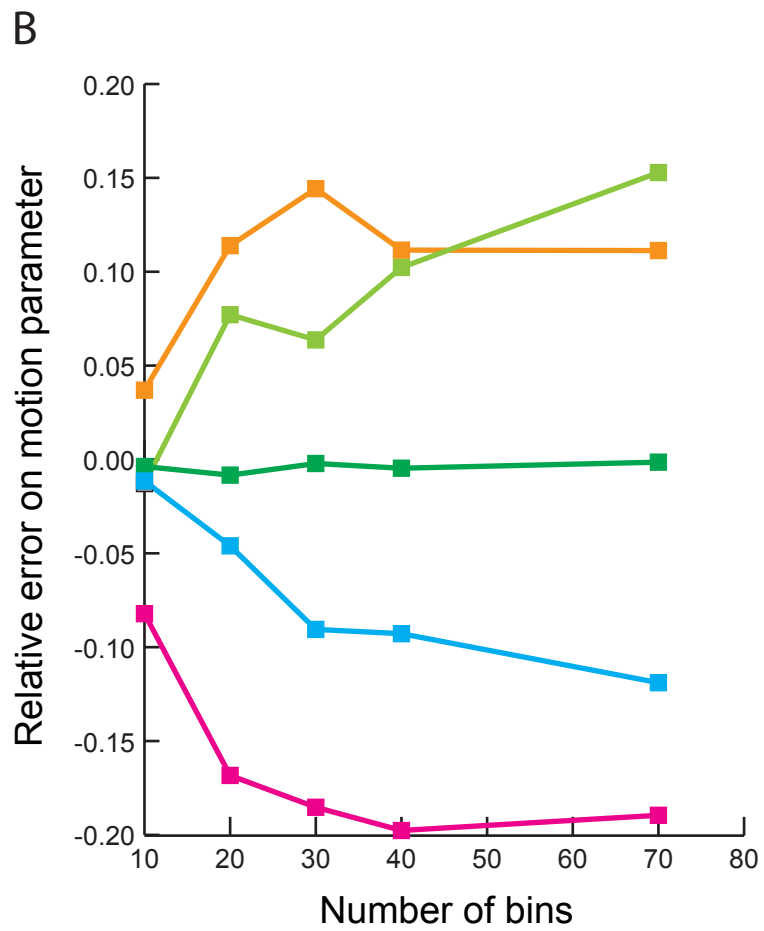
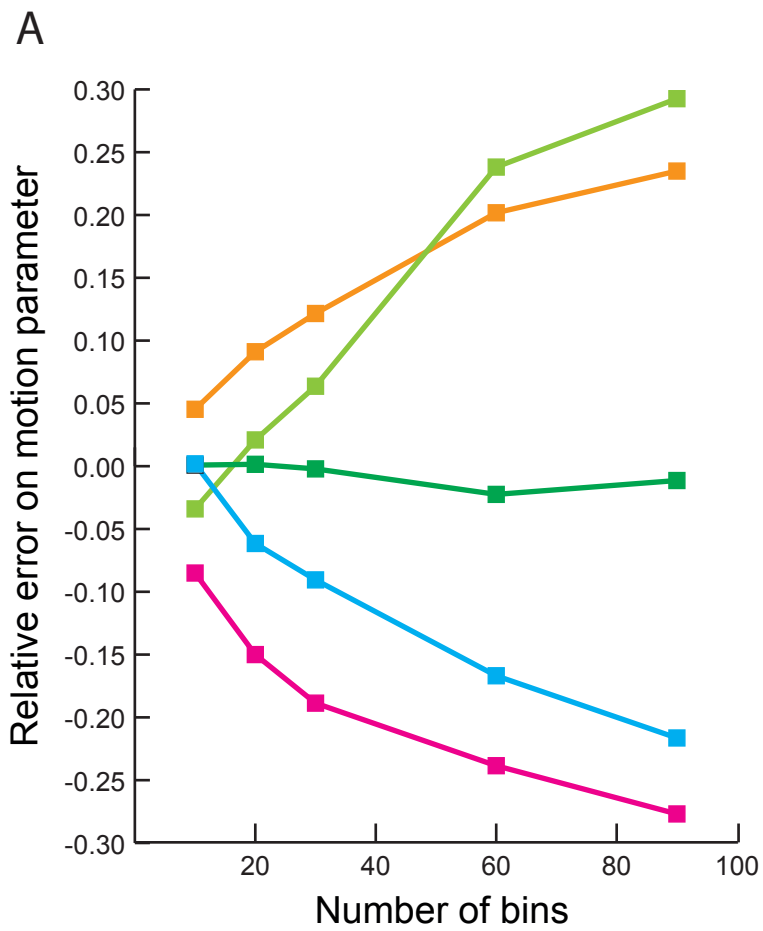
A

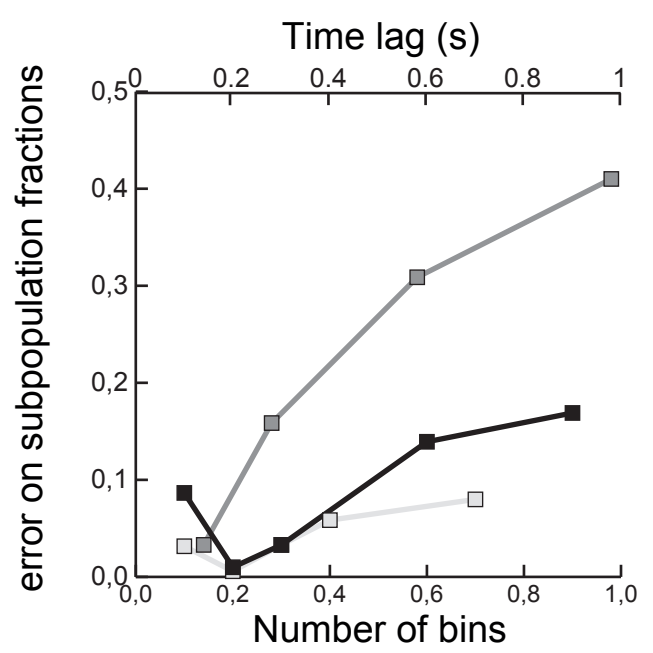
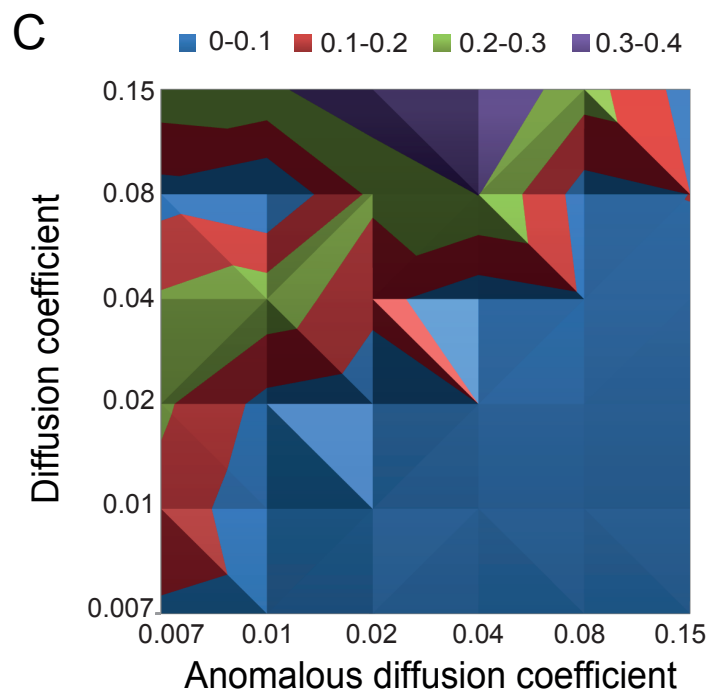
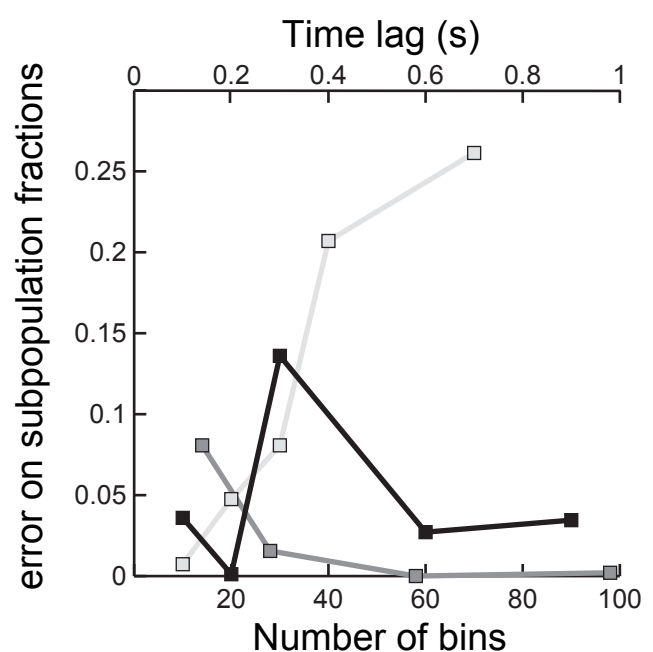
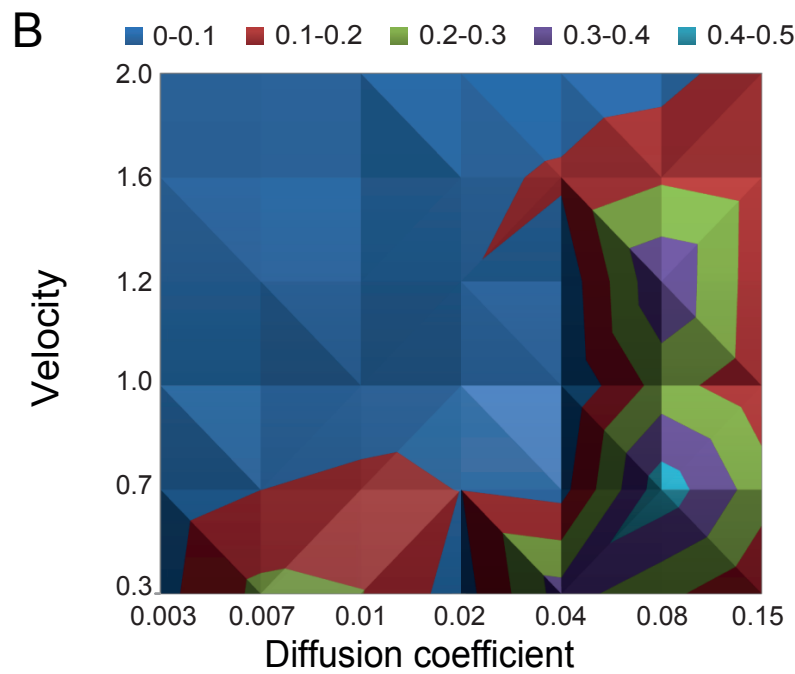
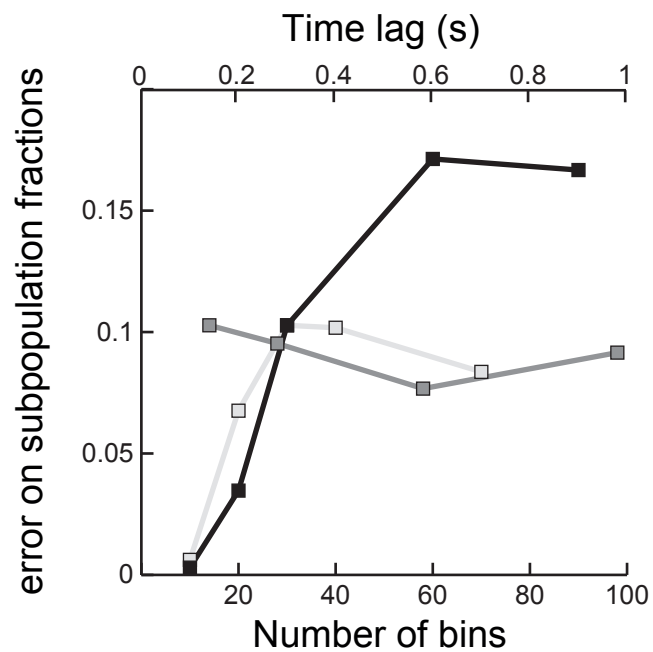
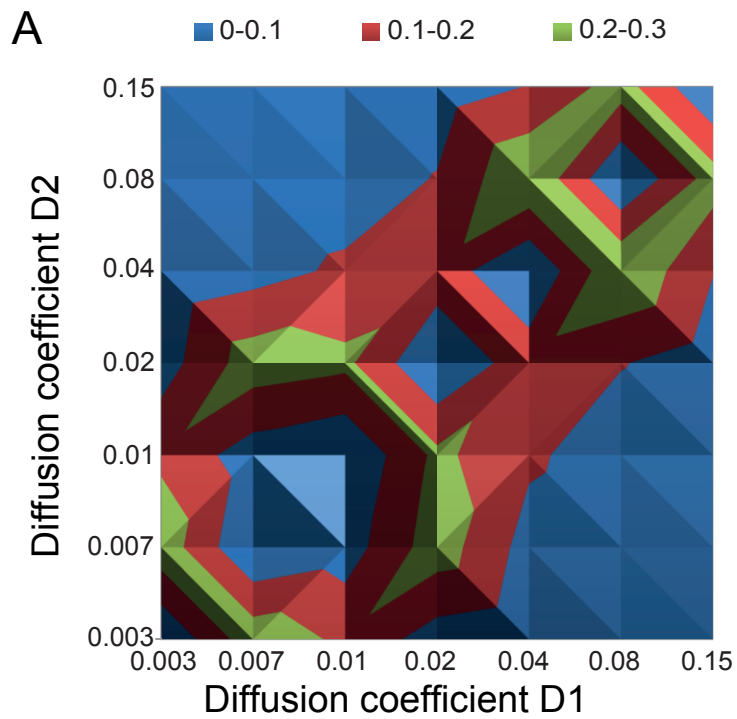
- Free diffusion (slow)
- Free diffusion (fast)
- Anomalous (sub)diffusion
- Directed transport



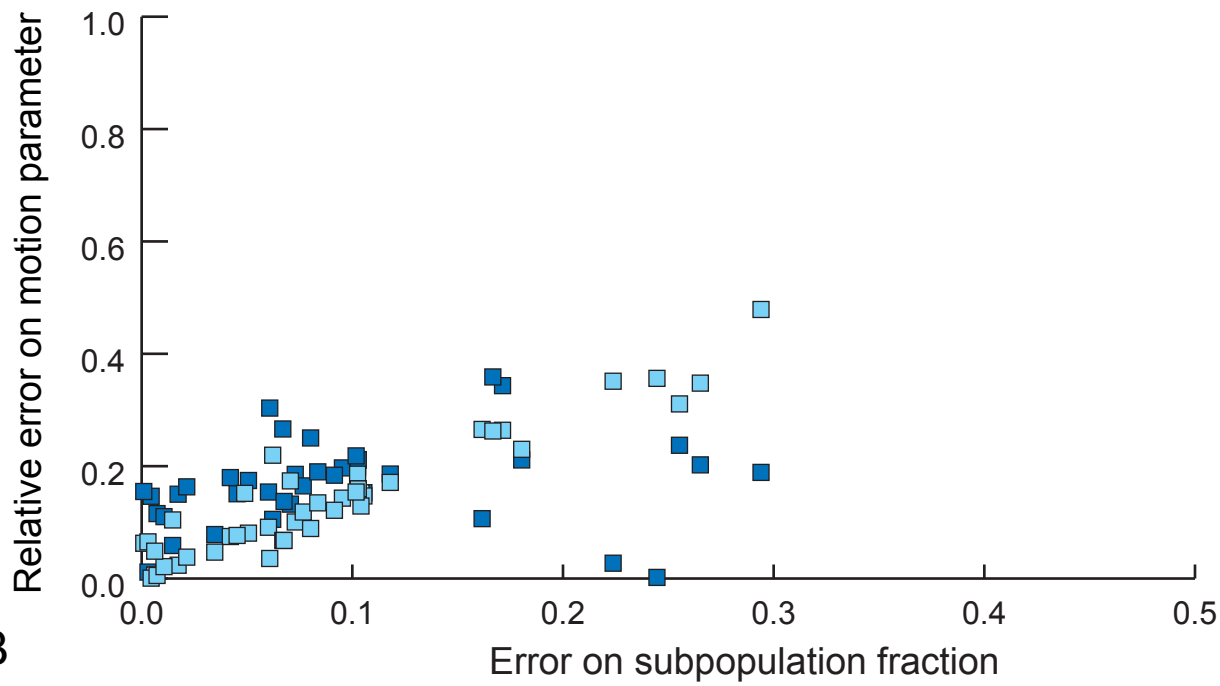
Individual molecule trajectories

B

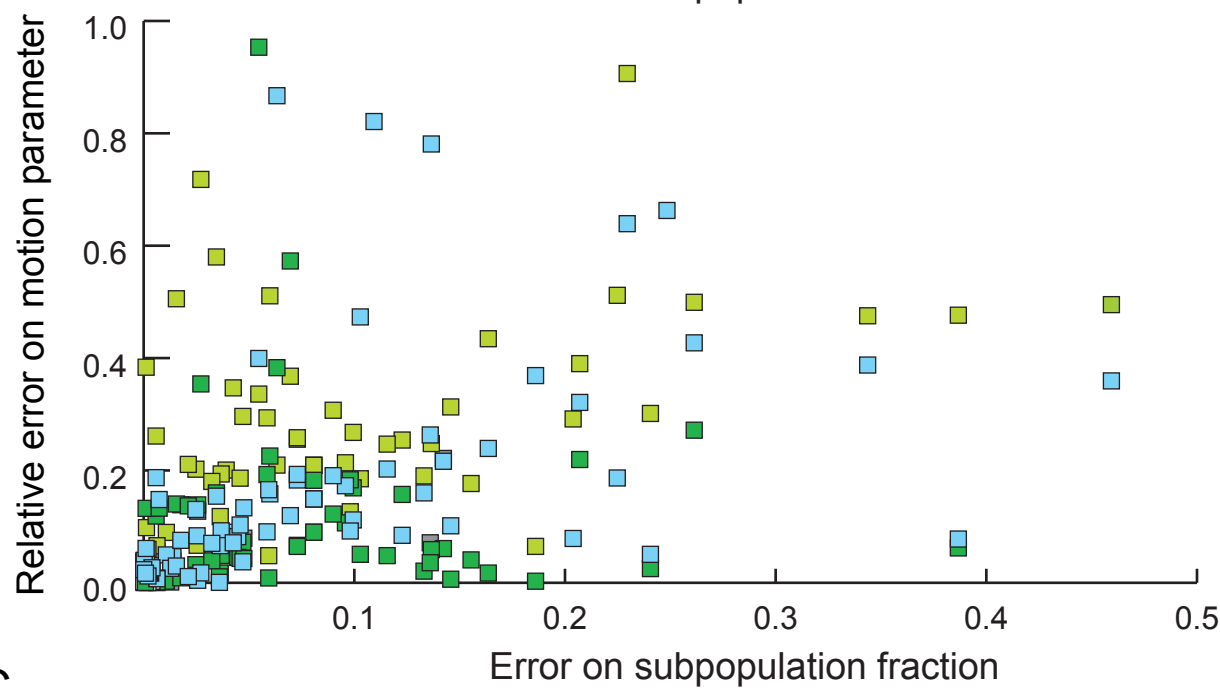




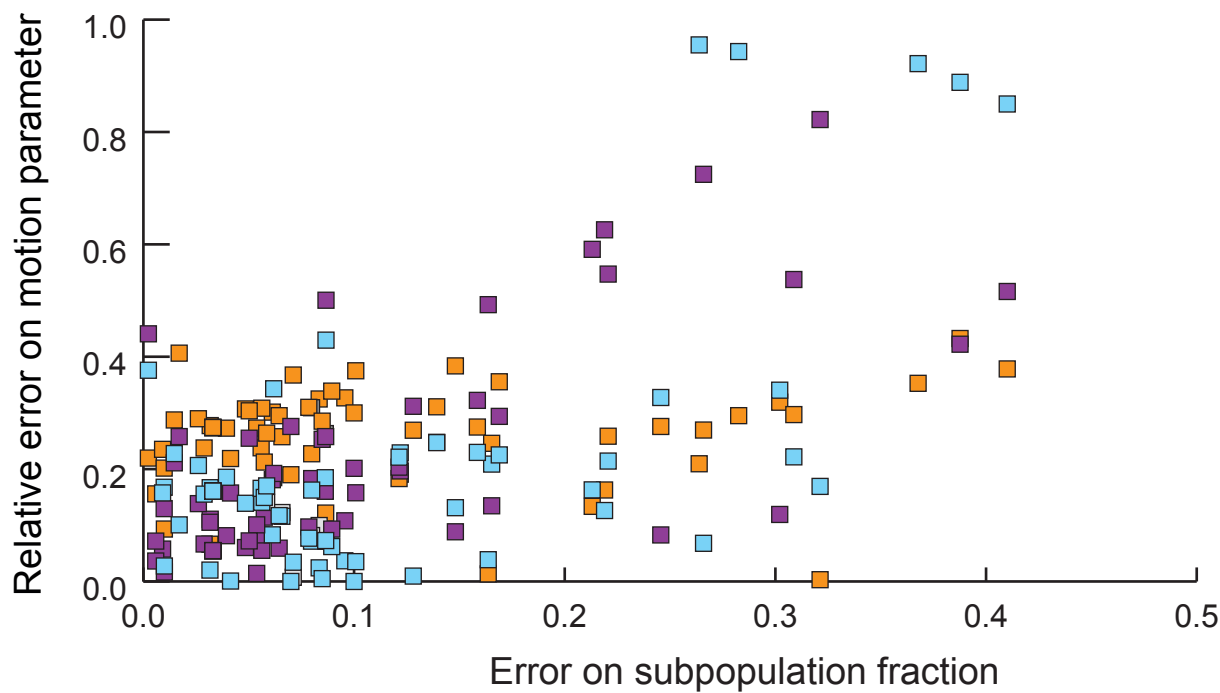
A



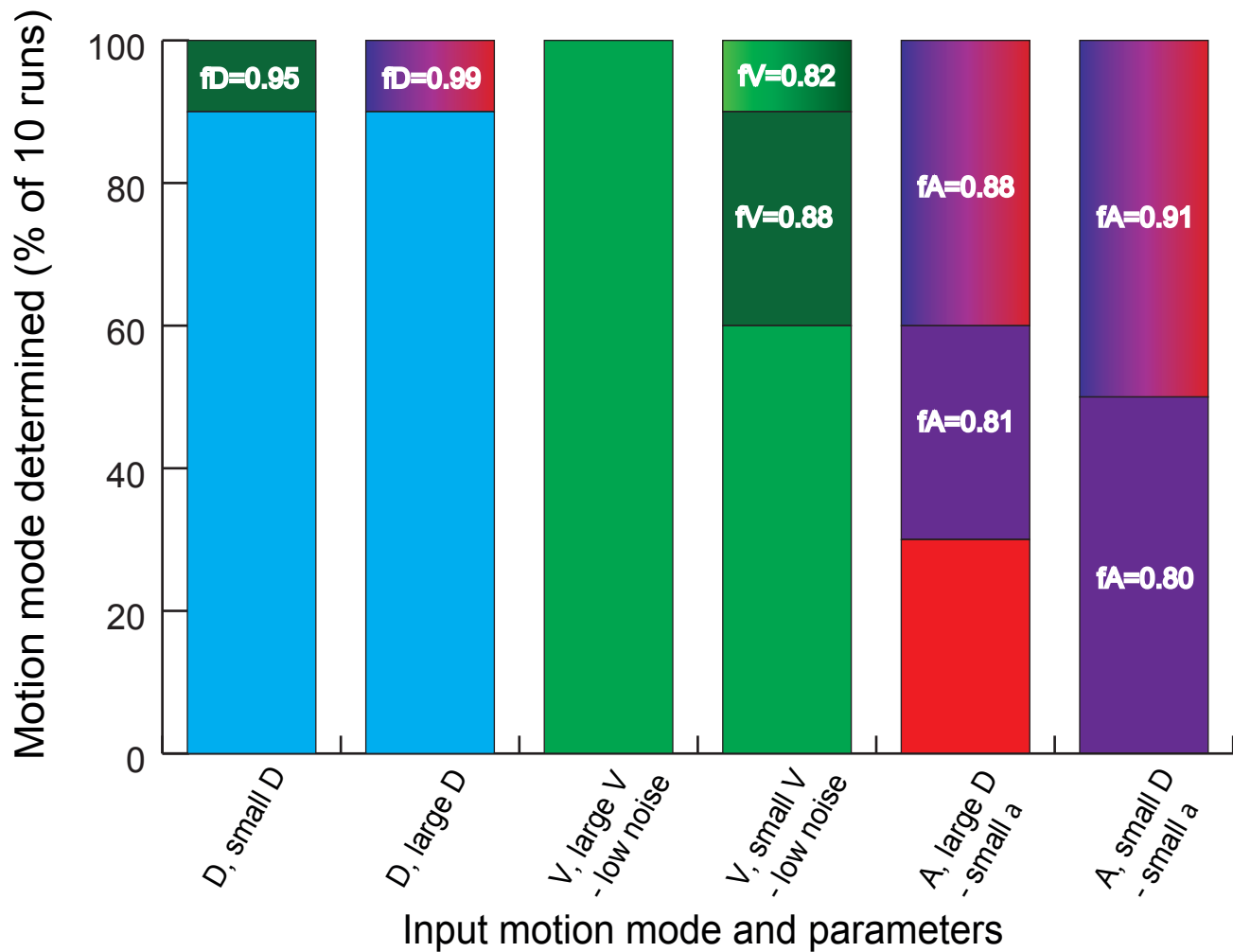
B



C



A



B

